Marine Geophysical Research (2021) 42:38
https://doi.org/10.1007/s11001-021-09457-7

ORIGINAL RESEARCH PAPER

Natural vs. trawling-induced water turbidity and suspended sediment transport variability within the Palamós Canyon (NW Mediterranean)

Marta Arjona-Camas[1,2] · Pere Puig[1] · Albert Palanques[1] · Ruth Durán[3] · Martin White[4,5] · Sarah Paradis[6] · Mikhail Emelianov[1]

Received: 3 June 2021 / Accepted: 12 September 2021 / Published online: 16 November 2021

Abstract

Increases of water turbidity and suspended sediment transport in submarine canyons have been associated with high-energy events such as storms, river floods and dense shelf water cascading (DSWC), and occasionally with bottom trawling along canyon flanks and rims. To assess the variations on the water column turbidity and sediment transport in the Palamós Canyon linked to both natural and trawling-induced processes, an autonomous hydrographic profiler, as well as a near-bottom current meter and a turbidimeter were deployed in the canyon axis (929 m depth) from February to June 2017, covering a trawling closure (February) and trawling activities (March-June). Periods of enhanced water turbidity during the trawling closure were mostly associated with storms and DSWC events, transporting turbid dense waters into the canyon. In absence of such events, the water column displayed low suspended sediment concentrations (~ 0.3 mg L^{-1}) until the trawling season began, when particulate matter detachments, ranging between > 1 mg L^{-1} and 3.8 mg L^{-1}, were observed at the water depths where the trawling grounds are found. During the trawling closure, high near-bottom suspended sediment fluxes (35–44 g m^{-2} s^{-1}) were sporadically registered at ~ 920 m depth associated with a major storm and DSWC event. Smaller but more frequent increases of near-bottom suspended sediment fluxes (0.1–1.4 g m^{-2} s^{-1}) were recorded during trawling activities. Despite these smaller trawling-induced suspended sediment fluxes, 30 days of continuous bottom trawling activity transported a total amount of 40 kg m^{-2}, of similar magnitude to that generated by a major DSWC event (50 kg m^{-2}). Since bottom trawling in Palamós Canyon is practiced on a daily basis throughout the year, a much larger contribution of anthropogenically derived water turbidity and suspended sediment transport can be expected.

Keywords Palamós Canyon · Dense shelf water cascading (DSWC) · Bottom trawling · Sediment transport · Nepheloid structure · NW Mediterranean

Introduction

Submarine canyons are widespread morphological features incising continental margins (Shepard and Dill 1966; Shepard 1972; Harris and Whiteway 2011) considered to be preferential pathways for the transference of water and sediments between nearshore areas and deep-sea environments (e.g., García et al. 2008; Allen and Durrieu de Madron 2009; Puig et al. 2014; Porter et al. 2016). For this reason, several studies have focused on studying the shelf-slope exchanges of downward particle fluxes and water turbidity by means of moored oceanographic instruments (see review by Puig et al. 2014). In these investigations, increases in sediment fluxes have been generally associated with lateral inputs of particulate matter by the action of different mechanisms such as breaking and/or shoaling of internal waves and tidal

✉ Marta Arjona-Camas
marjona@icm.csic.es

1 Institute of Marine Sciences (CSIC), Passeig Marítim de la Barceloneta, 37-49, 08003 Barcelona, Spain

2 Department of Earth and Ocean Dynamics, University of Barcelona, c/Martí i Franquès s/n, 08028 Barcelona, Spain

3 Marine Geology & Seafloor Surveying, Department of Geosciences, University of Malta, Msida, Malta

4 Earth and Ocean Sciences, Ryan Institute, National University of Ireland, Galway, Ireland

5 Irish Centre for Research in Applied Geosciences (iCRAG), Galway, Ireland

6 Geological Institute, ETH Zurich, Zurich, Switzerland

motions (e.g., Gardner 1989; Kunze et al. 2002; Cacchione and Ogston 2002; Puig et al. 2004b; Pomar et al. 2012) or high-energy storms affecting the upper portion of submarine canyons and hyperpycnal plumes formed during river floods (Monaco et al. 1990; Puig et al. 2004a; Palanques et al. 2006b, 2008; Bonnin et al. 2008; Ulses et al. 2008a). Occasionally, increases in turbidity have been associated with sediment gravity flow related events, such as slope failure on canyon walls (e.g., Paull et al. 2003; Puig et al., 2003, 2004a; Xu et al. 2004; Piper and Normark et al. 2009; Völker et al. 2011). Additionally, it has been demonstrated that dense shelf water cascading (DSWC) can also transport particles and erode and reshape the seafloor of submarine canyons, thereby increasing suspended sediment concentrations and transport towards the slope (Canals et al. 2006; Palanques et al. 2006b, 2008; Puig et al. 2008; Allen and Durrieu de Madron 2009). This later phenomenon is particularly relevant in the NW Mediterranean. Dense-shelf water formation tends to occur in winter over the Gulf of Lions (GoL) induced by dry and cold north and northwesterly winds (Tramontane and Mistral, respectively), which cause the cooling and heat loos of surface coastal waters. Eventually, these shelf waters become denser than the surrounding waters and sink over the shelf-edge and cascade downslope, mainly through submarine canyons until they reach their equilibrium depth, and continue flowing along the margin towards the southwest (Millot 1990; Durrieu de Madron 2005a). During mild or average winters, which are the most common in the study site, they are detached at intermediate depths, contributing to the formation of the seasonal Western Intermediate Water (WIW) found at the upper slope depths (Lapouyade and Durrieu de Madron 2001; Dufau-Julliand et al. 2004). In very dry, cold and windy winters, DSWC can be exceptionally intense, and dense shelf waters can affect the entire continental slope and even reach the basin floor (Canals et al. 2006; Palanques et al. 2012; Durrieu de Madron et al. 2013; Palanques and Puig 2018).

In addition to these various natural transport mechanisms, human activities, such as bottom trawling practiced at the flanks and rims of submarine canyons, have also been shown to contribute substantially to present-day sediment resuspension and water column turbidity (Palanques et al. 2006a; Puig et al. 2012; Martín et al. 2014a; Wilson et al. 2015b; Daly et al. 2018). Generally, the impacts of bottom trawling activities have been studied in shallow water environments, and mostly include the scraping and ploughing of the seabed by the use of heavy trawl doors that leave big furrows behind (Krost et al. 1990; Smith et al. 2003). The design of these heavy trawls also causes increases in near-bottom turbidity due to the sediment resuspension (O'Neill and Summerbell 2011), which contributes to the formation of turbid plumes and persistent nepheloid layers that are afterwards advected by local currents, waves and tides (Churchill 1989; Durrieu de Madron et al. 2005b; Palanques et al. 2001, 2014). However, shallow water environments on the continental shelf (< 120 m depth) are periodically impacted by natural sediment resuspension processes, masking the consequences of this anthropogenic activity. Therefore, assessing the relative contribution of oceanographic processes and anthropogenic activities to the sedimentary dynamics is rather complex because each area has its own wave climate, current regime, seabed sediment characteristics and bottom trawling frequency, and only a few studies have attempted to do this (e.g., Pilskaln et al. 1998; Churchill 1989; Ferré et al. 2008; Palanques et al. 2014; Oberle et al. 2016a; Mengual et al. 2016). A common conclusion of all these studies is that bottom trawling has a measurable impact on sediment resuspension in shallow-water environments, comparable to that created by natural forces. In deeper environments on the continental slope, however, bottom trawling disturbances can be more severe and have longer-lasting effects mainly because natural processes capable of overcoming human impacts are generally weaker than in shallower areas (Puig et al. 2012; Martín et al. 2014a; Oberle et al. 2016a).

The Mediterranean Sea hosts important deep-sea bottom trawl fisheries mainly located on the upper slope on the northwestern continental margin, where trawled bottoms exist up to 800 m depth, with greater depths being reached occasionally (Puig et al. 2012). Several studies aimed at understanding the effects of bottom trawling on the sediment dynamics in this area focused on the Palamós Canyon (also known as La Fonera or Llafranc Canyon) (Lastras et al. 2011), one of the most prominent morphological features incising this margin (Serra 1981). Some of these studies have shown that bottom trawling along the flanks of this canyon can trigger sediment gravity flows and transport sediments downslope from the fishing grounds to deeper regions of the canyon (Palanques et al. 2005; Martín et al. 2007, 2014a; Payo-Payo et al. 2017), affecting sediment accumulation rates in the canyon axis (Martín et al. 2006, 2008; Puig et al. 2015), and altering the natural morphology of the canyon flanks due to periodic reworking and removal of sediments (Puig et al. 2012). Additionally, Martín et al. (2014a) reported the presence of bottom and intermediate nepheloid layers (BNLs and INLs, respectively) in several hydrographic profiles conducted after the passage of the trawling fleet over the northern flank of the Palamós Canyon, but the continued effect of bottom trawling in this canyon causing changes in the water column turbidity beyond fishing grounds is an issue that remains largely unexplored.

Trawling-derived increases in suspended sediment concentrations (SSC) on the continental slope were also recorded in hydrographic studies conducted in the Celtic Sea (NE Atlantic). These studies showed unusual turbidity peaks in the water column within the Whittard Canyon that were linked to bottom trawling activities at the adjacent

canyon spurs (Wilson et al. 2015b; Daly et al. 2018). However, the temporal evolution of such trawling-induced turbidity increases throughout the water column has not been assessed in this submarine canyon. To our knowledge, the only study addressing this aspect in a trawled submarine canyon was conducted by Arjona-Camas et al. (2019) in the Foix Canyon (Catalan margin, NW Mediterranean). Two months of hydrographic profiles were acquired at the axis of this canyon during the trawling season, revealing the occurrence BNLs at the bottom of the canyon and quasi-permanent INLs over the canyon rim, originating from trawling activities on the adjacent continental slope. However, accurate estimates of the quantity of material being introduced by bottom trawling to the water column are still needed to better appreciate its contribution to the sediment dynamics and the potential environmental and ecological impacts associated with it. In this new study, we aim to assess the spatial and temporal variations on the water turbidity structure and near-bottom suspended sediment fluxes linked to both anthropogenic (bottom trawling) and natural (storms and DSWC) processes in the Palamós Canyon, as well as assess the contribution of each mechanism to the sediment fluxes.

Regional setting

The NW Mediterranean margin has a high density of submarine canyons, the Palamós Canyon (Fig. 1) being one of the most prominent examples (Canals et al. 2013). The canyon head is situated closest to the coastline at ~ 1 km and incises the continental shelf at 90 m depth. The first ~ 5 km of the canyon presents a N-S direction parallel to the coastline, after which the canyon's direction turns to WNW-ESE for ~ 35 km, separating the Roses margin to the north, and La Planassa margin to the south (Amblas et al. 2006). This submarine canyon has a total length of 110 km, and a maximum width of 18.4 km, and runs almost from the coastline down to 2550 m water depth. The canyon's steep walls (> 25º) present several well-developed gullies generated by sedimentary instabilities (Lastras et al. 2011), although these complex morphologies have been smoothened on fishing grounds due to recurrent disturbance of the seafloor by the trawling gear (Puig et al. 2012).

The hydrographic structure in this area is composed by a three-layer system (Salat and Cruzado 1981; Salat et al. 2002). Within the first layer, from the surface down to 150–300 m depth, the Atlantic Water (AW) is generally found. AW can be distinguished between "recent" and "old" according to the residence time in the Mediterranean basin that increases its salinity (Salat, 1996). In the NW Mediterranean, the oAW is found and is characterized by temperatures > 13 ºC and salinity values of 38.0–38.2. Mainly during wintertime, cold (~ 13 ºC) and fresh (~ 38.5) lenses of Western Intermediate Water (WIW) can be found at ~ 150 m depth. The second layer is formed by the Levantine Intermediate Water (LIW) between 300 and 600 m depth and is characterized by temperatures ~ 13.5 ºC and salinities of ~ 38.5. The third layer is formed by the near-homogeneous Western Mediterranean Deep Water (WMDW), which is formed in the open ocean resulting from intense sea-atmosphere heat exchanges and the subsequent buoyancy loss of offshore waters induced by cold, dry and persistent N-NW winds (Salat et al. 2002; Font et al. 2007). It covers the entire basin below 1000 m depth and has cold (~ 13 ºC) and salty (~ 38.5) characteristics (Font et al. 2007).

Since the Palamós Canyon is deeply incised in the continental shelf, it is capable of intercepting particulate matter transported by the Northern Current. This baroclinic current follows the continental slope from NE to SW in quasi-geostrophic equilibrium with a shelf-slope density front established between low-salinity coastal waters and the more saline and denser open waters (Font et al. 1988; Millot 1999). Although it approaches the Palamós Canyon mainly in a southwestward direction (Font et al. 1988), the abrupt topography of the canyon forces some adjustments of the Northern Current (Masó et al. 1991), which lead to significant vertical motions (Palanques et al. 2005; Jordi et al. 2005).

This submarine canyon also acts as a preferential conduit for particulate matter transported during sporadic events such as storms or river discharges (Palanques et al. 2005). The most important river in the nearby coast is the Ter River, whose mouth reaches the sea at 25 km north from the canyon. It has a mean annual water discharge of 12.1 $m^3 s^{-1}$ (Liquete et al. 2009). On this margin, northern storms are very frequent and persistent, but due to their reduced fetch they can only generate relatively small waves (~ 2 m) on the inner shelf that have limited capacity to resuspend sediment. Eastern storms are rarer and brief, although they generate larger waves (> 4 m), particularly during fall and winter months (Palanques et al. 2008). They are usually accompanied by heavy rains and torrential river discharges carrying large amounts of sediment to the coast (Ribó et al. 2011).

The Palamós Canyon's flanks are intensively exploited by a local trawling fleet targeting the blue and red shrimp *Aristeus antennatus*. Trawlers are active in this area on a daily basis except for weekends, holidays, and local festivities, mainly along the Sant Sebastià and the Rostoll fishing grounds (Fig. 1). The same vessel usually carries out two hauls per day, starting typically at 7 a.m. in an offshore direction, until 6 p.m. when it heads back to port. The average length of a haul usually ranges from 10 to 20 km, with

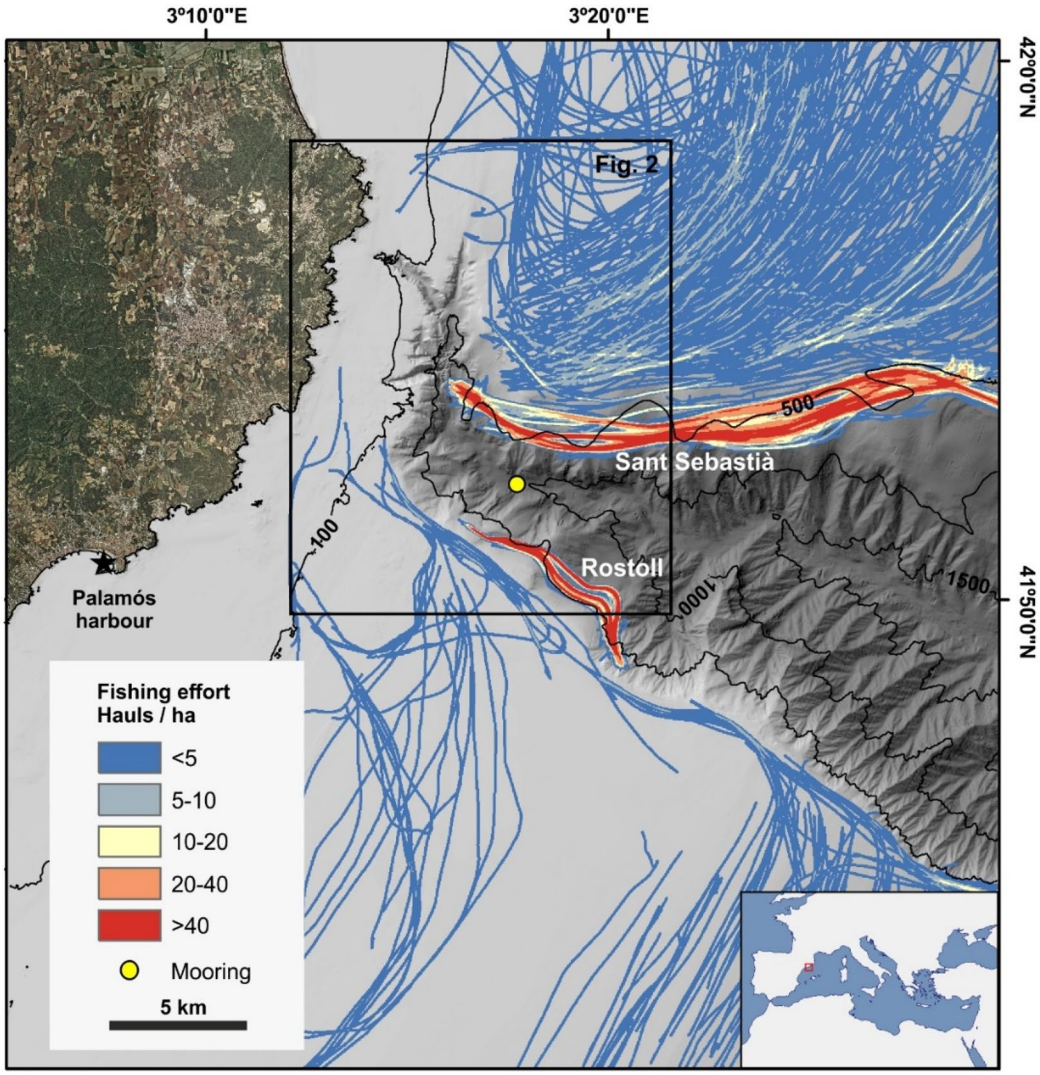

Fig. 1 Bathymetric map of the Palamós Canyon, showing the location of the mooring line in the canyon axis (yellow dot) and the main fishing grounds along the canyon flanks (Sant Sebastià and Rostoll). The overlying density represents an estimate of the fishing effort of otter board (OTB) vessels based on the number of hauls per hectare obtained from year 2017 Automatic Identification System (AIS) data. For interpretation of the references in color in this figure legend, the reader is referred to the web version of this article

an average of 15 km. The bottom trawl gear used in this fishery consists of two heavy otter boards, each up to 1 ton in weight, spreading ~ 100 m apart during the trawling operation and connected to the net opening by 60–200 m long sweeplines. The net measures 80–150 m in length and has a width of ~ 50 m at its ballasted mouth (Palanques et al. 2006a; Martín et al. 2014a). A recent fishery management established a two-month trawling closure from early-January to early-March since 2013 to allow the recruitment of juveniles and avoid the risk of overexploitation of the fishing stock (Bjørkan et al. 2020). In 2017, this seasonal trawling closure occurred from January 5 to March 8 (BOE 2017).

Materials and methods

Moored instruments

During the oceanographic cruise ABIDES-1, onboard the R/V *García del Cid*, a mooring line was deployed in the axis of the Palamós Canyon at 929 m depth (41° 52.329′ N;

3º 7.660′ E), at a slightly deeper location than the maximum working depth of the local trawling fleet (~ 800 m) (Fig. 1). One of the main concerns when deploying instruments in a trawled submarine canyon is the risk of losing data and expensive instrumental as a result of a collision with fishing gear. During this study, the position and deployment depth of the mooring was chosen in agreement with the Palamós fishermen guild in order to avoid interfering with their bottom trawling activities, and still be able to carry out our experimental observations in the canyon. The deployment was programmed from February 7 to early June, 2017, which covered a trawling closure period (February) and the continuation of the regular trawling season in the fishing grounds of the canyon (March-June). Unfortunately, the instruments recorded good data during 60 days until April 7, when the mooring line was displaced by a longline fishing vessel from a neighboring fishing harbor. Nevertheless, the recorded period allowed to capture the transition between the fishing closure and the trawling season and to address the scientific goals pursued in this study.

Autonomous hydrographic profiler

The mooring line was equipped with an autonomous hydrographic profiler (Aqualog) programmed to perform two up- and down-casts per day (at 2 a.m. and 2 p.m.), at a relative speed of 0.25 m s^{-1}, from ~ 150 to 738 m water depth (parking position). Therefore, the upper ~ 150 m and the lower ~ 200 m of the water column at the mooring location were not monitored. Unfortunately, the Aqualog did not profile the entire water column at certain time spans during the study period (i.e., February 7–27), presumably caused by the tilting of the mooring line due to strong currents, which prevented the carrier from progressing deeper and completing the hydrographic profiles.

The profiler was equipped with a SeaBird 19 plus CTD probe configured to collect temperature, salinity and pressure at 4 Hz (i.e., 4 scans per second). The profiler was also equipped with a SeaPoint turbidity sensor, programmed to measure water turbidity in Formazin Turbidity Units (FTU) by detecting scattered light from suspended particles at 0–25 FTU range, at 1 Hz (i.e., 1 scan per second).

Near-bottom instrumentation

The lower portion of the mooring line was also equipped with a single point Nortek Aquadopp current meter coupled with a SeaBird SBE-37 placed at 6 m above the bottom (mab) at 923 m depth that provided data at 5-min sampling interval. Closer to the bottom (at 5 mab), the mooring line also sustained an AQUA-logger 210TY equipped with a SeaPoint turbidity sensor that measured at 1-min sampling interval. The logger was set to operate in autogain mode, allowing to measure turbidity readings up to 2000 FTU.

CTD transect

After the mooring recovery, on June 7, 2017, a ship-based hydrographic transect was conducted in the study area onboard the R/V *García del Cid*. The transect consisted in 15 vertical stations across the canyon head, collected using a SeaBird 911 CTD probe coupled with a SeaPoint turbidity sensor (see location in Fig. 2).

Data analysis

Suspended sediment concentration

FTU readings from the CTD probes and moored instruments were converted into suspended sediment concentration (SSC) units using a regression equation obtained from a laboratory calibration. It was carried out by deploying eight different AQUA-logger 210TY SeaPoint turbidity sensors in an experimental tank, in which suspended particulate matter, using bottom sediments that were previously collected at the

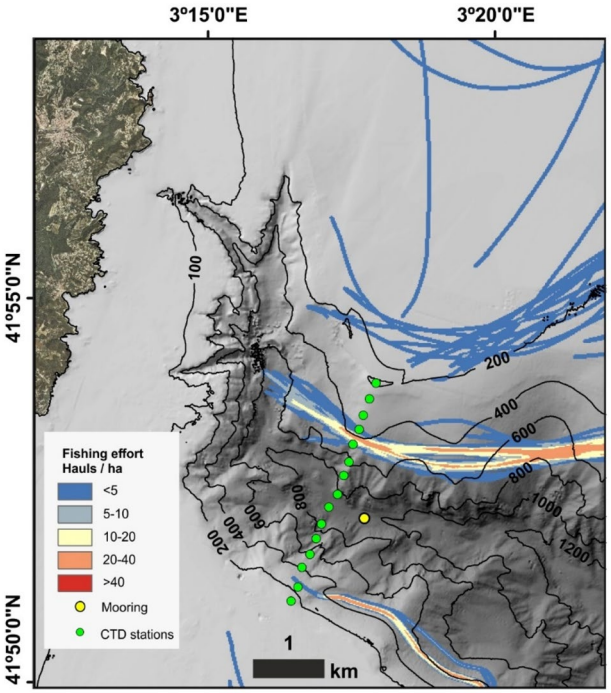

Fig. 2 Bathymetric map of the Palamós canyon head showing the fishing effort between March 9 and April 7, 2017 (trawling season). The yellow dot depicts the location of the mooring line, while the green dots indicate the position of the hydrographic transect conducted in June 7, 2017. For interpretation of the references in color in this figure legend, the reader is referred to the web version of this article

study site, was introduced incrementally. With continuous stirring, water samples were taken at given FTU readings and filtered through pre-weighed Nucleopore membranes to obtain SSC values, yielding the following linear regression (Fig. 3):

$$SSC\left(\text{mg}\cdot L^{-1}\right) = 1.14\cdot FTU - 0.37\ \left(r^2 = 0.99\right)$$

Net particulate standing crop

The SSC profiles obtained by the Aqualog were used to compute the Net Particulate Standing Crop (NPSC, mg cm^{-2}) by calculating the excess over the value of the clear water minimum and integrating the SSC excess over the height of the profiling range:

$$NPSC = \frac{1}{h}\int_0^h SSC(z)dz$$

where h stands for the depth of the considered water column (in m) and SSC (z) represents the estimated SSC (in mg L^{-1}) (see details in Karageorgis and Anagnostou 2003; Arjona-Camas et al. 2019).

As the profiler did not reach the same depths during the trawling closure and the trawling period, two distinct approaches were considered. In the first one, the NPSC was calculated for the 150–400 m depth interval, where data was recorded throughout the deployment period. In the second, the NPSC was computed only for the time-period when the profiler recorded data along most of the working depth range (150–738 m depth).

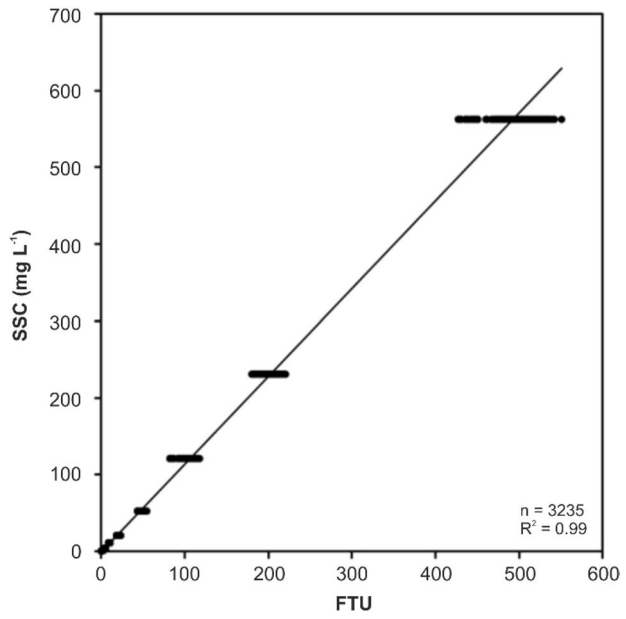

Fig. 3 Relation between the turbidity signal (FTU) and the measured suspended sediment concentration (SSC, mg L^{-1}) for the eight turbidity sensors used in this laboratory calibration

Sediment fluxes

Near-bottom currents and SSC data were used to calculate instantaneous suspended sediment fluxes, as well as time-integrated cumulative suspended sediment transport at each timestep (i), following:

$$Flux_i = V_i \times C_i = current_i \times SSC_i$$

where current speed_i, in m s^{-1}, multiplied by SSC, in mg L^{-1}, yielded to instantaneous suspended sediment flux in g m^{-2} s^{-1}.

Then, the time integrated cumulative suspended sediment transport (in kg m^{-2}) can be calculated following:

$$Cumulative\ transport = \sum_{i=1}^{N} Flux_i \times\ \Delta t = Sum\ of\ flux_i\ x\ time\ step$$

where the timestep was 5 min (or 300 s), corresponding to the measuring interval of the near-bottom current meter placed at 923 m depth. This multiplied by the instantaneous suspended sediment flux yielded to the time-integrated cumulative suspended sediment transport.

An intermediary computation prior to calculating sediment flux and cumulative transport is needed to estimate the current components with respect to geographical coordinates by applying an angle Θ of rotation. In our study, to obtain the along- and across-canyon components at the mooring location, the North and East current components were rotated 70 degrees counterclockwise based on the canyon axis orientation.

For the along-canyon component up-canyon fluxes are positive, whereas for the down-canyon fluxes are negative. For the across-canyon component NE orientation fluxes are positive, whereas SW fluxes are negative. The integration of the instantaneous suspended sediment fluxes for the duration of the study period yields the cumulative across- and along-canyon suspended sediment transports.

Long time series have an uncertainty associated to errors on the measurement of the different variables, which deserve to be calculated to complete sediment flux and time-integrated cumulative transport calculations. These uncertainties are derived from measurements of particle concentration derived from turbidity, as well as the propagation error along the time series. Hence, for any measure on a time series, we have an uncertainty on both along- and across-canyon current components (σ_v), an uncertainty on suspended sediment concentration (σ_c), and an uncertainty on suspended sediment fluxes (σ_F) and time-integrated cumulative transport (σ^2_{NF}). Estimated parameters' uncertainties derived from the measurement errors corresponding to each independent

time series are shown in Table 1. The uncertainty (or error propagation) in suspended sediment fluxes, for each time step, can be calculated following:

$$\sigma_F^2 = \left(\frac{\partial F}{\partial Speed}\right)^2 \times \sigma_{Speed}^2 + \left(\frac{\partial F}{\partial Dir}\right)^2 \times \sigma_{Dir}^2 + \left(\frac{\partial F}{\partial Turb}\right)^2 \times \sigma_{Turb}^2$$

$$\begin{aligned}\sigma_F^2 &= ([A \times Turb] \times cos(90 - Dir + \theta))^2 \times \sigma_{Speed}^2 \\ &+ (-Speed \times [A \times Turb] \times sin(90 - Dir + \theta))^2 \times \sigma_{Dir}^2 \\ &+ \left(A \times \left[Speed \times cos(90 - Dir + \theta)\right]\right)^2 \times \sigma_{Turb}^2\end{aligned}$$

The uncertainty associated to time-integrated cumulative transport (NF) is calculated following:

$$\sigma_{NF}^2 = \Delta t^2 \times \sum_{i=1}^{N} \sigma_{Flux_i}^2$$

Assessment of fishing effort

The activity of bottom trawlers around the Palamós Canyon operating in the fishing grounds of Sant Sebastià (northern canyon flank) and Rostoll (southern canyon flank) (Fig. 1) was obtained from ShipLocus®, the main module of the Spanish Ports Authority to exploit maritime traffic data for management and research purposes (Puertos del Estado 2017), through the use of Automatic Identification System (AIS) tracking. Vessels with AIS provide their position omni-directionally at intervals that can vary from 2 s to 3 min to nearby AIS-bearing ships, as well as to coastal stations and satellites, enabling the monitoring of fine-scale vessel behaviors and movement patterns (Natale et al. 2015).

The spatial fishing effort was estimated using AIS data from year 2017, which included the study period, and consisted in static data of fishing vessels (vessel name, call sign identifier, IMO number, dimensions) and their dynamic data (vessel position, speed over ground, course over ground and heading). Since the total volume of AIS dataset exceeded computational dataset management capacities, the dataset was reduced to the first entry per minute of each vessel. This resulted in a smaller and homogeneous dataset for the study period. Vessels equipped with otter trawl boards (OTB) were extracted by cross-checking the AIS dataset with data from the Community Fishing Fleet Register (European Commission Fisheries and Maritime Affairs 2014). AIS data were then filtered according by speed to infer whether an AIS message corresponded to fishing activity, using similar criteria to those used in previous studies (e.g., Natale et al. 2015; Oberle et al. 2016a; Paradis et al. 2021). It assumes that bottom trawler speed follows a bimodal distribution corresponding to navigating (high speed) and trawling (low speed) conditions. Trawling speed was finally obtained as the mean of the first gaussian distribution ± 2 standard deviations (95 % of the distribution) of the OTB vessel speeds. This interval corresponds to speeds between 0.8 and 3.9 knots. However, simply filtering according to this trawling speed may lead to false-positives, when a trawler is navigating or drifting at a specified trawling speeds, and false-negatives, when a trawler is hauling at anomalous speeds for a few minutes due to piloting reasons (i.e., when trawling down-slope the vessel needs to reduce its speed to keep the gear on the seafloor). Hence, a minimum length of 10 min per haul was assumed to correct for false-positives, whereas anomalous speeds that lasted less than 5 min were considered to correct for false-negatives. Hauls per vessel were then defined as consecutive entries that met these trawling criteria for at least 100 min.

Finally, bottom trawling effort was obtained from the total number of hauls within one hectare (100 × 100), assuming an average trawling-door spread of 100 m. These units are a good indicator of the times that a trawler tows an area and can be used as a proxy of their capacity to resuspend bottom sediments (Ragnarsson and Steingrimsson 2003; Martín et al. 2014b). Trawling effort was finally represented and plotted using ArcGIS© 10.4 software for the entire monitoring period (Fig. 1), and for the trawling closure (spanning from February 7 to March 8) and for the trawling season (spanning from March 9 until the end of the study period on April 7) (Fig. 2).

Table 1 Estimated parameters' uncertainties derived from the measurement errors to each independent time series. The variance of the variables as well as constant parameters are shown. "A" corresponds to the constant that multiplies FTU values to yield SSCs, while Θ corresponds to the angle of rotation applied to obtain along- and across-canyon currents. In this case, $\Theta = 70º$, with respect to the North and East components, is applied in the equations for uncertainty calculations

Variable	Variance/constant	Value
Current speed	σ_{Speed}	± 0.005 m s^{-1}
Current direction	σ_{Dir}	$\pm 5º$
Turbidity	σ_{Turb}	± 2.7 FTU
Constant of turbidity	A	1.14
Angle of rotation (counter-clockwise)	Θ	70º

Ancillary data

The daily discharges of the Ter and the Daró rivers, located slightly northwards of the Palamós Canyon, were supplied by the Agència Catalana de l'Aigua (Catalan Government Water Agency), and have been used to assess the riverine sediment supplies during the study period. This data is available online via ACA's website (http://aca-web.gencat.cat/sdim21/seleccioXarxes.do).

Wave conditions during the study period were provided by the REDEXT network of deep-water oceanographic buoys of the Spanish Ports Authority (http://www.puertos.es/es-es/oceanografia/Paginas/portus.aspx) and recorded hourly by the Cap de Begur buoy, located offshore on the northern continental slope region next to Palamós Canyon, over the 1200 m isobath (41° 55.2′ N; 3° 39.0′ E).

Results

Activity of OTB vessels

The fishing grounds of the Palamós canyon were exploited by 34 OTB vessels, most of which from the Palamós harbor, but occasionally from Blanes and Roses harbors (located southwards and northwards, respectively, and not shown in Fig. 1).

Time-series observations on OTB vessel positions, based on fishing effort, revealed no trawling activity occurred around the mooring site during the trawling closure at the flanks of the canyon (not shown), while during the trawling season, the fishing effort increased on both canyon flanks (Fig. 2). In the Rostoll fishing ground section located closer to the mooring and CTD transect, bottom trawling occurred at relatively shallow depths ranging from 250 to 450 m, at a predominating frequency of 5 hauls per hectare. The fishing effort in the Rostoll fishing ground increased seawards, reaching 10–30 hauls per hectare at 500–600 m depth. At the Sant Sebastià fishing ground, the predominating frequency in the canyon wall next to the mooring and the CTD transect was 20–40 hauls per hectare between 400 and 800 m depth (Fig. 2). The number of daily hauls was computed at both fishing grounds during the monitored trawling season, being generally higher in Sant Sebastià than in Rostoll, and accounting for a total of 74 hauls against 31 hauls, respectively (Fig. 4).

More scattered trawling activity was also observed on the upper continental slope at depths < 200 m (Fig. 2). This fishing effort was estimated to be less than 5 hauls per hectare during the monitored trawling season. The number of hauls computed at these depths was considerably smaller in comparison to those computed at the depths of the canyon flanks' fishing grounds and accounted for a total of 18 hauls for the monitored trawling season (Fig. 4).

Forcing conditions

During the monitoring period, several storms, defined as sustained significant wave heights (Hs) greater than 2 m for more than 6 h (Mendoza and Jiménez 2009), were recorded during the monitoring in early February, and early- and late-March, the majority of them caused by strong northern winds and with Hs > 3 m (Fig. 5a). These events were generally dry storms (Guillén et al. 2006) that did not lead to significant increases in Ter and Daró River discharges (Fig. 5b).

Four major storms (Hs > 4 m) were recorded during the monitoring period. A strong northern storm occurred in early February with maximum Hs of 4.9 m, which lasted more than 15 h (Fig. 5a). A unique strong eastern storm with maximum Hs of 4.7 m at the peak of the storm that lasted from February 12 to February 16 (Fig. 5a) caused a torrential Ter River discharge that reached 30.6 $m^3\ s^{-1}$ on February 15, concurrent with a small increase of 6.0 $m^3\ s^{-1}$ at the Daró River (Fig. 5b). A stronger northern storm with a maximum Hs of 5.1 m occurred on March 4 that lasted for

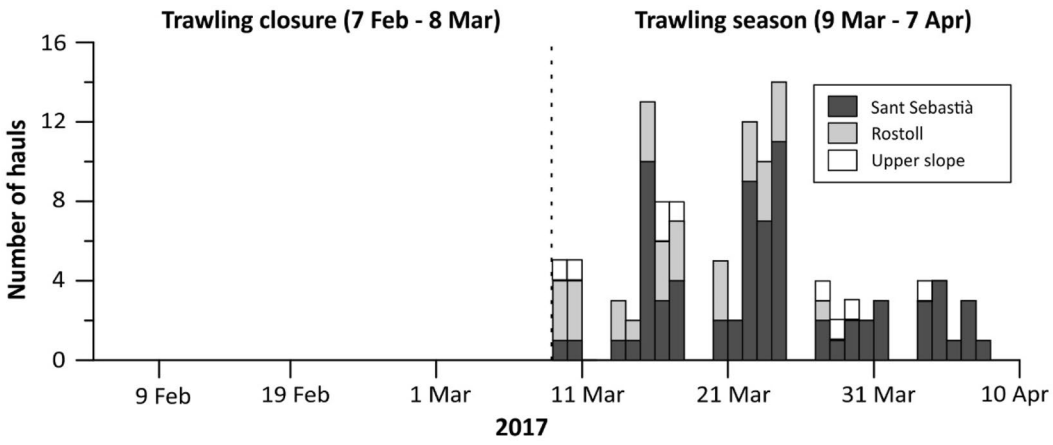

Fig. 4 Daily hauls in the Sant Sebastià and Rostoll fishing grounds, and in the upper slope region during the monitoring period. The dashed line separates the trawling closure from the trawling season

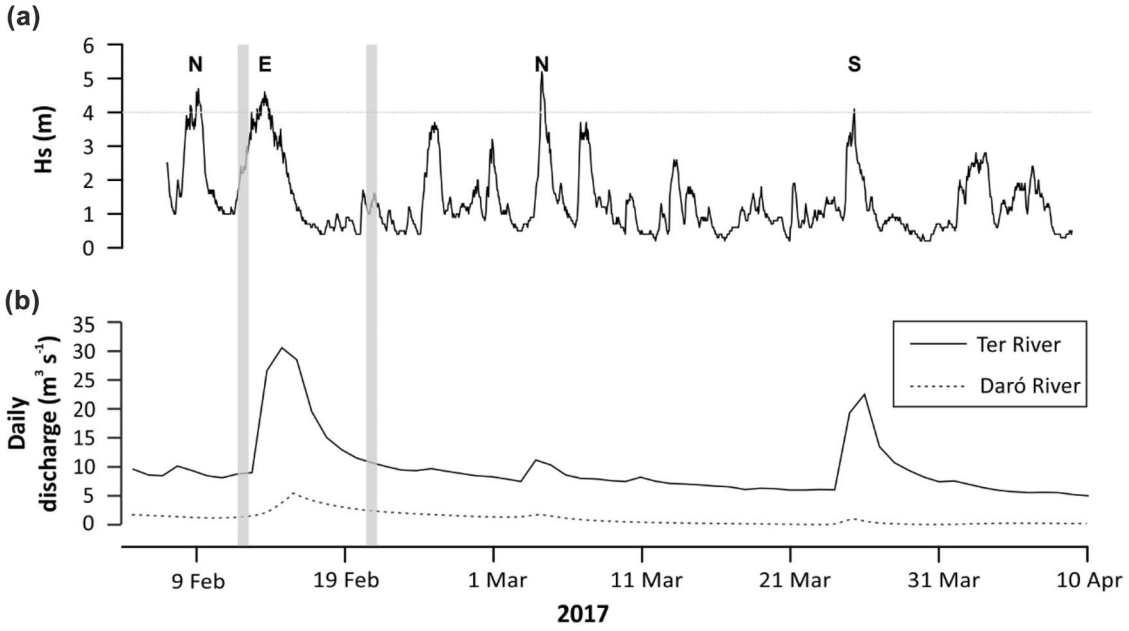

Fig. 5 Temporal evolution of the **a** significant wave height (*Hs*, m) measured at the Cap de Begur buoy and **b** the Ter and the Daró river discharges ($m^3\ s^{-1}$) during the monitoring period. Major storms, with Hs > 4, are indicated with an N (northern storms), E (eastern storms) or an S (southern storms) according to their origin. The occurrence of dense shelf water cascading (DSWC) events is indicated by a grey vertical bar

two days (Fig. 5a) and led to a Ter River discharge of 11.1 $m^3\ s^{-1}$ and a Daró River discharge of 2.2 $m^3\ s^{-1}$ (Fig. 5b). At the end of the study period, a strong southern storm with maximum Hs of 4.1 m occurred on March 25 (Fig. 5a), which lead to a Ter River discharge of 19.4 $m^3\ s^{-1}$ and a Daró River discharge of 1.5 $m^3\ s^{-1}$ (Fig. 5b).

Time series observations

Identification of water masses

Compiled data of all hydrographic profiles during the monitoring period revealed distinct changes in temperature and salinity throughout the water column that are ascribed to the different water masses in the study area (Fig. 6).

The old Atlantic Water (oAW) occupied the shallowest water column (150–300 m) during most of the recording period (Figs. 6 and 7). Below oAW, the temperature and salinity time series, as well as the Θ-S diagram, showed the more saline Levantine Intermediate Water (LIW), mainly centered at 500–600 m water depth (Figs. 6 and 7). The Western Mediterranean Deep Water (WMDW) was generally observed at the deepest part of the hydrographic profiles, exhibiting its characteristic temperature and salinity values (Figs. 6 and 7). In addition to these water masses, the seasonal Western Intermediate Water (WIW, Θ = 12.9–13.2 ºC; S = 38.1–38.3) and two pulses of Dense Shelf Water (DSW), displaying temperature minima reaching < 12.6 ºC along with salinity values < 38.2,

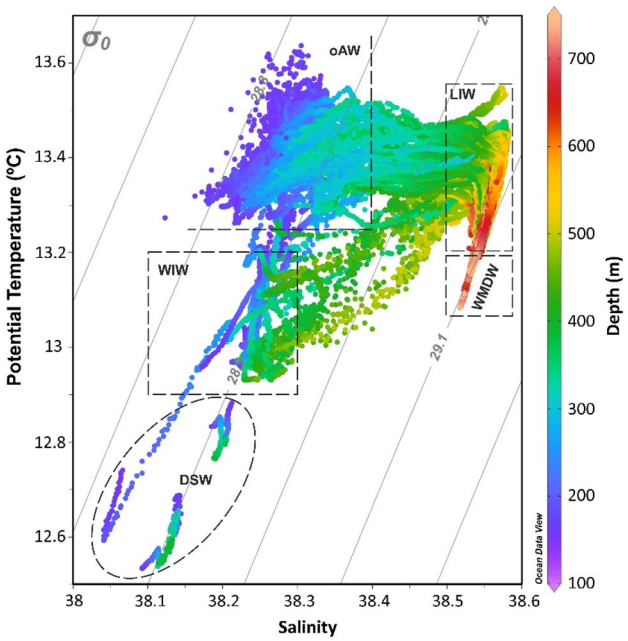

Fig. 6 General Θ-S diagram for all the hydrographic casts acquired by the autonomous hydrographic profiler (Aqualog) during the monitoring period identifying the different water masses in the study area: oAW (old Atlantic Water), WIW (Western Intermediate Water), DSW (Dense Shelf Water), LIW (Levantine Intermediate Water), WMDW (Western Mediterranean Deep Water). For interpretation of the references in color in this figure legend, the reader is referred to the web version of this article

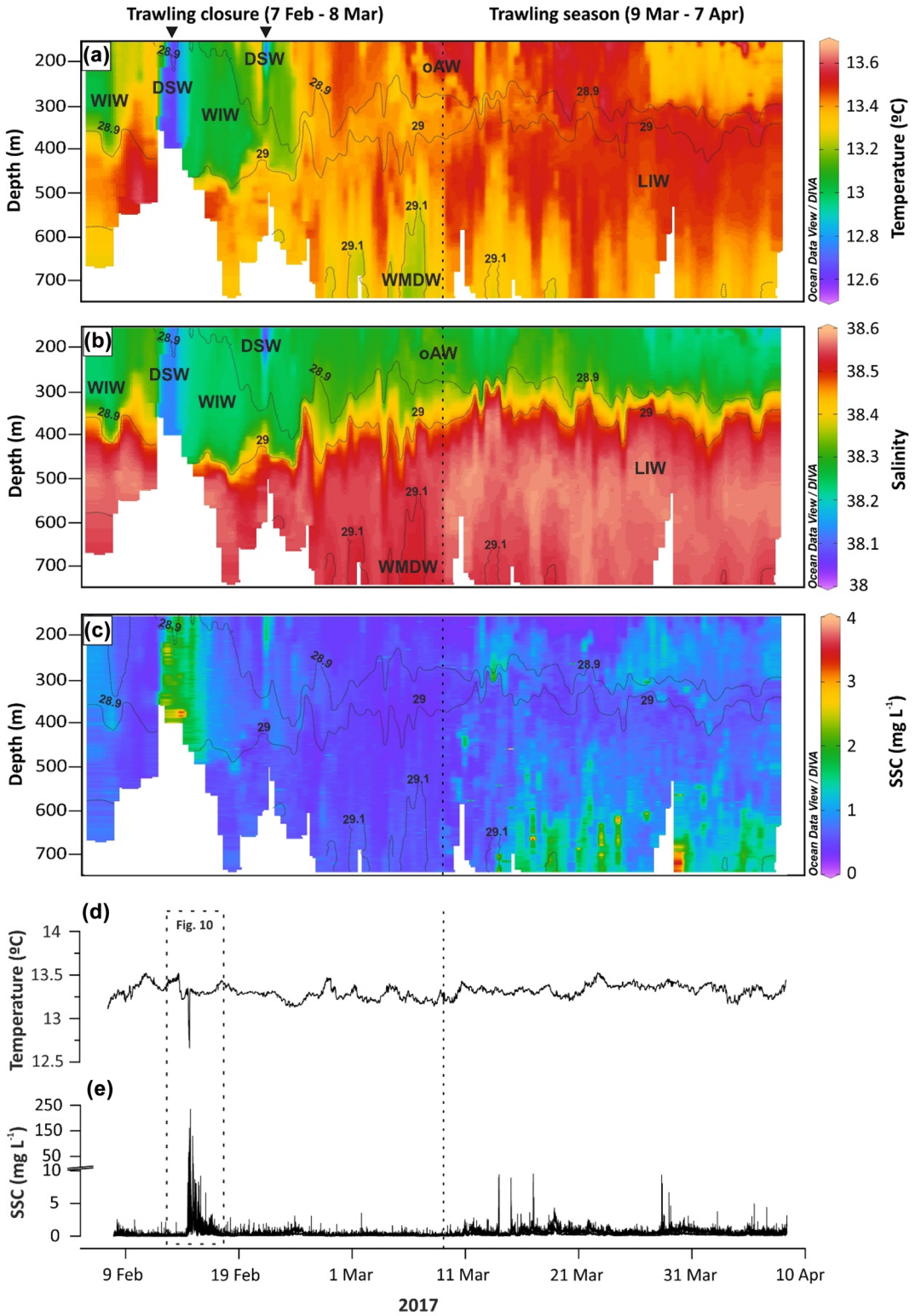

Fig. 7 Time series of **a** temperature (ºC) **b** salinity, and **c** suspended sediment concentration (SSC, mg L^{-1}) measured by the autonomous hydrographic profiler (Aqualog), as well as **d** temperature (ºC) and **e** SSC measured by the near-bottom instrumentation during the monitoring period. Panels a and b show the different water masses being present in the study area: oAW (old Atlantic Water), WIW (Western Intermediate Water), DSW (Dense Shelf Water), LIW (Levantine Intermediate Water), WMDW (Western Mediterranean Deep Water). The occurrence of two dense shelf water cascading (DSWC) events is indicated by a black triangle. Blank spaces represent incomplete profiles. The dashed line separates the trawling closure from the trawling season. For interpretation of the references in color in this figure legend, the reader is referred to the web version of this article

were observed at the beginning of the recording period (Figs. 6 and 7). Particularly, the presence of DSW and WIW over the Palamós Canyon occurred from February 7 to February 24, the latter mainly ranging from 150 to ~400 m depth (Fig. 7a, b).

Evolution of water column suspended sediment concentration (SSC)

The vertical particulate matter distribution showed increasing SSC (up to 1 mg L^{-1}) that lasted for the first two days of the monitoring period, in agreement with the presence of WIW (Fig. 7c). Immediately afterwards, the water turbidity decreased and maintained values < 0.8 mg L^{-1} in the profiled water column for 6 days, when water turbidity increased to between 1.1 and 3.8 mg L^{-1} from February 13 to February 15 coinciding with the first DSW pulse into the canyon (Fig. 7a–c) (see the first black triangle). This DSWC event was noted by a sharp decrease in temperature (~0.5 ºC) and salinity (~0.2) values (Fig. 7a, b). This first pulse of DSW was detected all along the entire profiling range recorded at that time. However, it was only observed reaching depths between 370 and 400 m in the hydrographic profiles recorded by the Aqualog, without being able to capture its deeper limit in these profiles (Fig. 7a-c). This DSW pulse reached the canyon axis, as observed by the temperature and turbidity values recorded close to the bottom by the near-bottom instrumentation, presenting near-bottom temperatures of ~12.6 ºC (Fig. 7d) and maximum SSC of ~234 mg L^{-1} (Fig. 7e). Afterwards, water turbidity maintained relatively high SSCs along the hydrographic profiles for three days associated with the presence of WIW, ranging from 0.4 to 1.1 mg L^{-1} down to depths of ~500 m (Fig. 7c). On February 21, the shallowest part of the hydrographic profiles recorded a new decrease in temperature and salinity values, and an increase of SSC of 2.2 mg L^{-1}, coinciding with the arrival of the second pulse of DSW into the canyon (Fig. 7a-c). However, it only lasted for a few hours and descended to maximum water depths of 200 m (see the second black triangle), without displacing the WIW found underneath (Fig. 7a, b). After this event, and until February 24, the vertical particulate matter distribution still showed events of moderate SSC elevation in the water column that ranged between 0.3 and 0.9 mg L^{-1} from the uppermost part of the hydrographic profiles to maximum water depths of 500 m (Fig. 7c). From February 24 to the end of the study period, the WIW was absent and recorded temperature and salinity values that corresponded to the more general hydrographic structure of the northwestern Mediterranean, with the presence of surface oAW, the core of LIW at mid-waters and centered between 500 and 600 m and the WMDW occupying the deeper part of the profiled water column (Fig. 7a, b). During this period, the vertical distribution of particulate matter showed no periods of significant SSC increase in the profiled water column until the beginning of the trawling season on March 9 (Fig. 7c).

During the trawling season, several SSC increases were recorded at intermediate waters (from 150 to 300 m depth), reaching up to 2.5 mg L^{-1} and at the lower part (> 500 m depth) of the profiled water column (Fig. 7c). A relative clear water minimum was recorded between 300 and 500 m water depth. The maximum SSC was recorded on March 30 at ~718 m depth, reaching up to 3.8 mg L^{-1} (Fig. 7c). Near-bottom time series (923 m depth) of temperature and turbidity values remained constant during most of the time, displaying temperature values ranging from 13.2 to 13.6 ºC (Fig. 7d) and SSC < 1.5 mg L^{-1} (Fig. 7e). Punctual increases in SSC between 5 and 10 mg L^{-1} were recorded during the trawling season (Fig. 7e), although such increases showed no relation with temperature fluctuations.

The NPSC for the upper part of the profiled water column peaked at ~40.7 mg cm^{-2} and 23.3 mg cm^{-2} during the two DSW pulses, respectively (see black triangles in Fig. 8a), and decreased to baseline NPSC values (~10 mg cm^{-2}) at the end of the closure season. The NPSC values increased again in the trawling season, when almost a double-fold increase in the NPSC (~20 mg cm^{-2}) was observed (Fig. 8a). In the second approach, considering the entire profiling range, the NPSC varied between 8.3 and 20.8 mg cm^{-2} during the end of the closure season, whereas it was doubled and even quadrupled during the trawling period, reaching maximum values of 50.1 mg cm^{-2} (Fig. 8b).

Near-bottom currents

During most of the recording period, near-bottom currents followed the canyon axis (Fig. 9a, b). Current speeds varied between 0.05 and 0.25 m s^{-1} during most of the monitoring in both along- and across-canyon directions (Fig. 9c, d), although periodic reversals in the current direction mainly oriented up- and down-canyon were observed (Fig. 9c).

This general current pattern was altered between February 14 and February 15, during the first DSW pulse, when near-bottom currents and SSC changed drastically (Figs. 9 and 10). During the first stages of this event, temperature experimented a slight increase of 0.2 ºC (Fig. 10a), concurrent with an increase of the down-canyon current velocity up to 0.2 m s^{-1} (Fig. 10b) but slightly oriented towards the NE sector (Fig. 10c), while turbidity progressively increased up to 75 mg L^{-1} (Fig. 10d). A sharp decrease in near-bottom temperature (~0.5 ºC) reaching down to 12.6 ºC (Fig. 10a) was recorded afterwards and, simultaneously, currents reached speeds of 0.3 m s^{-1} with dominant down-canyon direction but oriented towards the SW (Fig. 10b, c), while near-bottom turbidity increased up to 160.1 mg L^{-1} (Fig. 10d). Three hours later, the temperature increased to 13.3 ºC (Fig. 10a), which was

concurrent with a maximum peak in current speed up to 0.6 m s^{-1} directed up-canyon (Fig. 10c). When this current reversal occurred, a sharp increase in turbidity was observed, reaching maximum SSC of ~ 234 mg L^{-1} (Fig. 10d). Near-bottom currents maintained the up-canyon flow direction for almost 5 h (Fig. 10b), and turbidity values gradually decreased to 4 mg L^{-1} (Fig. 10d). Afterwards, the near-bottom current flow reversed following the down-canyon direction (Fig. 10b) and slightly towards the SW (Fig. 10c). Another current reversal of up to 0.3 m s^{-1} was detected up-canyon (Fig. 10b), while another concurrent important turbidity peak of 96 mg L^{-1} was recorded (Fig. 10d). Towards the end of this event, the current speed and turbidity decreased to baseline values (Fig. 10b–d).

Near-bottom suspended sediment fluxes and cumulative transport

During most of the trawling closure, instantaneous along-canyon near-bottom suspended sediment fluxes fluctuated between 0.02 and 0.1 g m^{-2} s^{-1} (Fig. 11a) and between 0.01 and 0.06 g m^{-2} s^{-1} in the across-canyon direction (Fig. 11b). However, during the first DSWC pulse, there was an increase in both along- and across-canyon suspended sediment fluxes. In the along-canyon direction, suspended sediment flux increased up to 19 g m^{-2} s^{-1} down-canyon, but the more important suspended sediment flux was registered up-canyon, reaching values of 44 g m^{-2} s^{-1} (Fig. 11a). In the across-canyon direction, suspended sediment flux increased up to 8.8 g m^{-2} s^{-1} towards the NE, although the maximum suspended sediment flux was registered towards the SW reaching up to 35 g m^{-2} s^{-1} (Fig. 11b). The cumulative transport after this event was up-canyon (Fig. 11c) and towards the SW (Fig. 11d), reaching values of 50 kg m^{-2} and 80 kg m^{-2}, respectively.

During the trawling season, near-bottom instantaneous along-canyon suspended sediment flux ranged from 0.1 to 0.7 g m^{-2} s^{-1} and was predominantly in the up-canyon direction, and across-canyon suspended sediment flux reached maximum values of 1.4 g m^{-2} s^{-1} mainly towards the SW (i.e., coming from the northern flank) (Fig. 11a, b). Therefore, throughout the trawling season, the resultant cumulative suspended sediment transport was in the up-canyon direction and from the northern canyon flank (towards the SW) in the across-canyon component, reaching 40 kg m^{-2} and 20 kg m^{-2}, respectively (Fig. 11c, d).

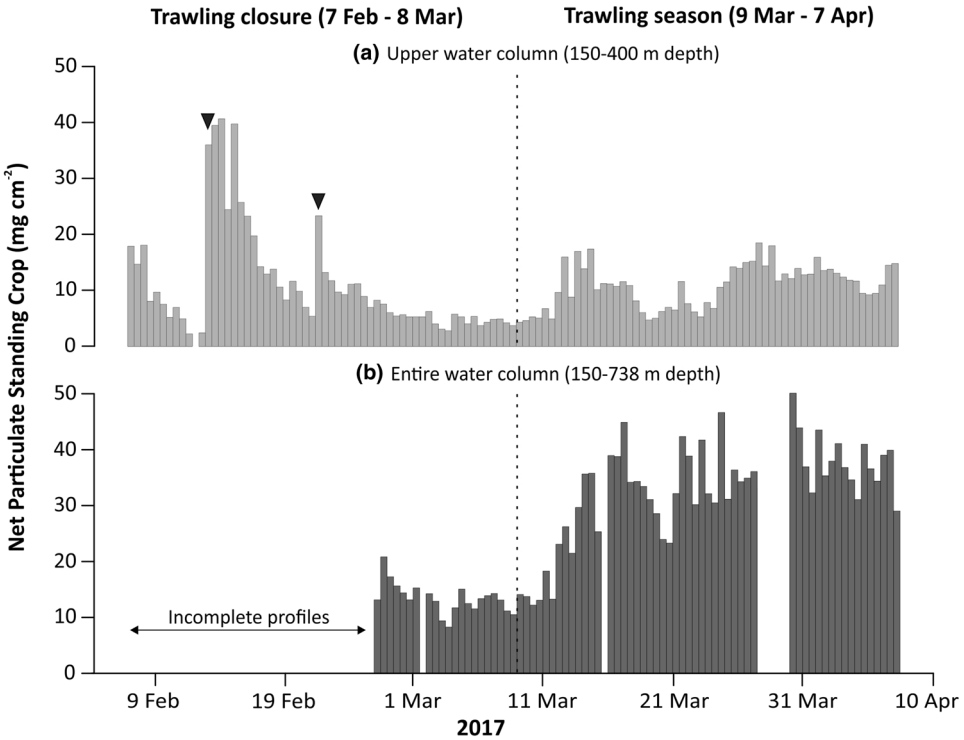

Fig. 8 Net Particulate Standing Crop for **a** the upper water column (150–400 m depth) and for **b** water depths between 150 to 738 m depth during the monitoring period. The occurrence of two dense shelf water cascading (DSWC) events is indicated by a black triangle. The dashed line separates the trawling closure from the trawling season

CTD transect

The hydrographic data obtained by the June 7, 2017 high-resolution CTD transect across the Palamós canyon head from the surface down to 925 m water depth revealed distinct changes in temperature and salinity throughout the water column (Fig. 12). In the first 50 m of water column, waters with distinctly low salinities (38.0-38.2) and high temperatures (15–19 ºC) were observed (Fig. 12a, b), most probably corresponding to the influence of the seasonal thermocline. The signature of the oAW, characterized by temperatures > 13 ºC (Fig. 12a) and salinity values ranging from 38.0 to 38.4 (Fig. 12b), was found underneath, reaching water depths down to 200 m in the northern canyon flank and ~ 300 m in the southern canyon flank. Below (down to ~ 800 m water depth), the temperature and salinity along the transect showed the more saline LIW core, which displayed a salinity maximum (S > 38.5) centered ~ 500 m water depth (Fig. 12a, b). The deepest part of the water column was occupied by the WMDW that exhibited temperature minima of 13 ºC and salinity values of 38.5 (Fig. 12a, b).

SSC distribution across the studied canyon section showed a surface clear water layer down to ~ 100 m water depth and a continuous INL with concentrations ~ 0.5 mg L^{-1} extending over the entire canyon width in the water parcel occupied by the oAW (Fig. 12c). Within the canyon confinement, the central part of the water column mainly corresponded to the upper levels of the LIW core and was characterized by low SSC, whereas near-bottom waters in both canyon flanks and close to the canyon axis displayed higher SSC. Over the southern canyon wall, there was a detachment of a thin BNL mainly centered at

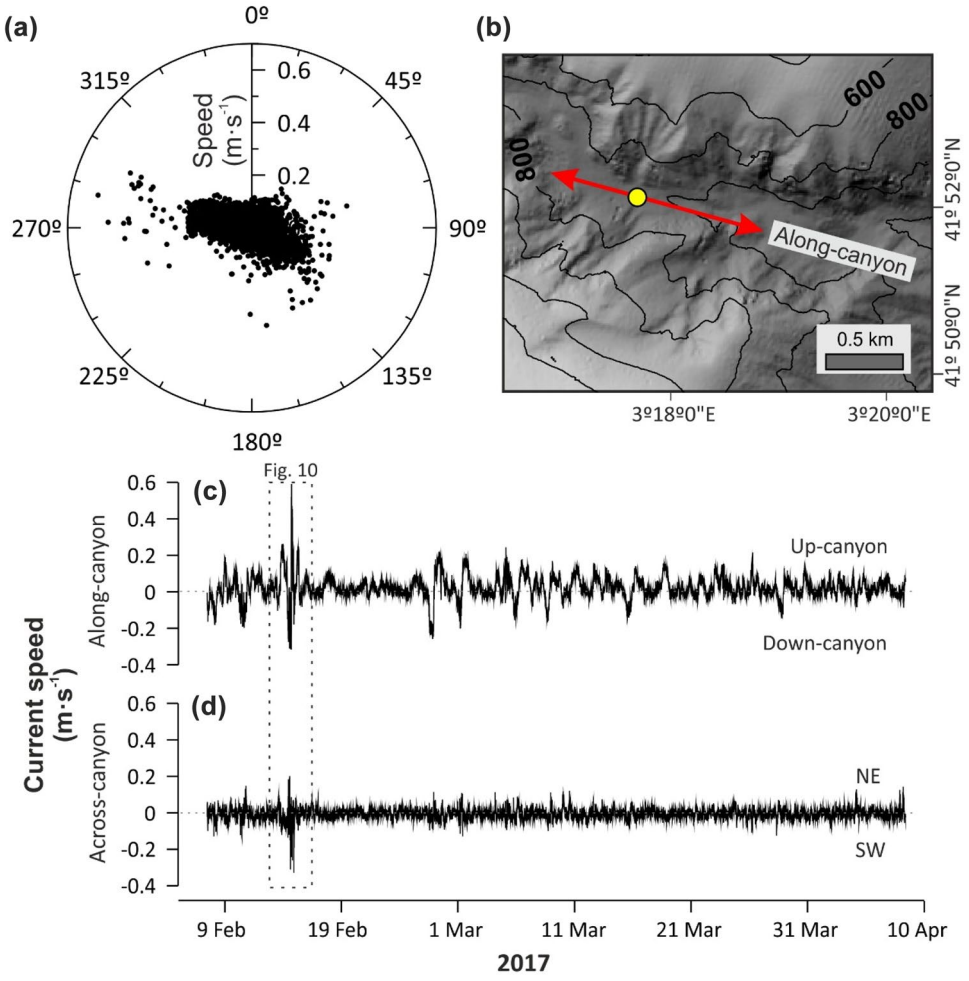

Fig. 9 Near-bottom currents during the monitoring period. **a** Polar plot of current speed and direction showing the preferential current orientation. **b** Close-up of the bathymetry at the mooring location (yellow dot) and the canyon axis orientation used to rotate the current velocity components (red arrow). Panels **c** and **d** correspond to the time series of along-canyon current velocity and across-canyon current velocity components, respectively

~ 300 m depth, reaching SSC up to 3 mg L^{-1} (Fig. 12c, station #2). This detachment extended ~ 450 m horizontally towards the canyon interior as an INL, which was observed in station #3 at the same water depth, but with SSC values of 0.5 mg L^{-1}. On the northern canyon wall, a well-developed BNL displaying SSCs up to 1.5 mg L^{-1} was observed at ~ 450 m water depth (Fig. 12c, station #11), which evolved towards the canyon interior and to a less concentrated and thicker BNL, with SSC ~ 1 mg L^{-1} extending from 550 to 700 m depth (Fig. 12c, station #10). The lower part of the profiled water column over the canyon axis (stations #5 to #9) showed SSC > 0.5 mg L^{-1} that corresponded to scattered and isolated INLs showing poor lateral continuity among consecutive hydrographic casts (Fig. 12c).

Discussion

Natural-induced water turbidity and suspended sediment transport

The earlier studies using moored instrumentation demonstrated that river floods and storms enhanced particle fluxes inside submarine canyons and on the continental slope (Monaco et al. 1990; Puig and Palanques 1998b), and for a long time, these processes were considered the major contemporary mechanisms able to transport sediments from shallow water environments to deeper environments. Recent studies conducted in the NW Mediterranean also recognize the importance of the formation of dense shelf waters and their subsequent downslope cascading, exporting sediment

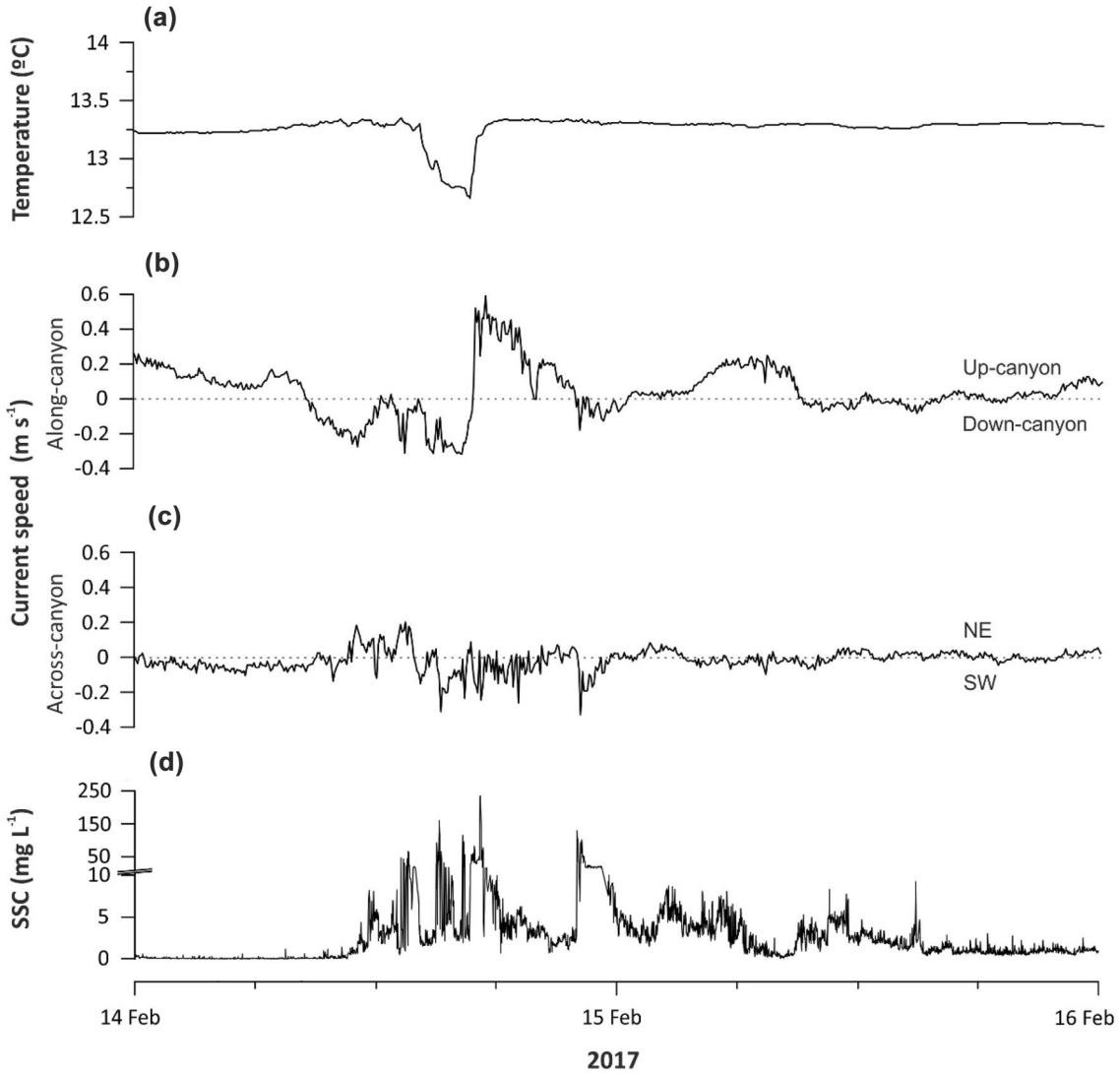

Fig. 10 Time series of near-bottom **a** temperature (ºC), **b** along-canyon current velocity (m s^{-1}), **c** across-canyon current velocity (m s^{-1}), and **d** suspended sediment concentration (SSC, mg L^{-1}) measured during the first DSWC event

particles towards deep-sea regions (Canals et al. 2006; Palanques et al. 2006a). DSWC events occur frequently, preferentially during early winter, after a period of several months without significant storms during which the continental shelf can be covered by easily resuspendable sediment from nearby rivers.

In the Palamós Canyon, Ribó et al. (2011) reported for the first time the presence of DSWC events related to eastern storms. In this investigation, priority was given to the deployment of near-bottom instruments at the canyon head, on the assumption that most of the suspended sediment transport and water turbidity increases were coming from the shelf and relatively confined near the canyon seafloor. The results presented in this new study contribute to refine the sediment dynamics associated to DSWC events in the Palamós Canyon providing additional information throughout the water column, as well as near the bottom at a deeper canyon axis location (Figs. 7, 8, 9, 10 and 11). During the present study, the first DSWC event was enhanced by a major eastern storm that occurred between February 12 and February 16, which also led to a torrential water discharge from the Ter River. The eastern storm was most probably responsible for the expulsion of dense coastal waters on the shelf upstream of the canyon, which alongside with the ephemerally sediment deposited on the shelf by the Ter River, generated high downslope and down-canyon sediment transport into Palamós Canyon. The DSW signal was detected along the profiled water column from 150 to 377 m depth and also near the bottom at 923 m depth (Fig. 7), which suggests an increase of turbidity throughout the entire water column.

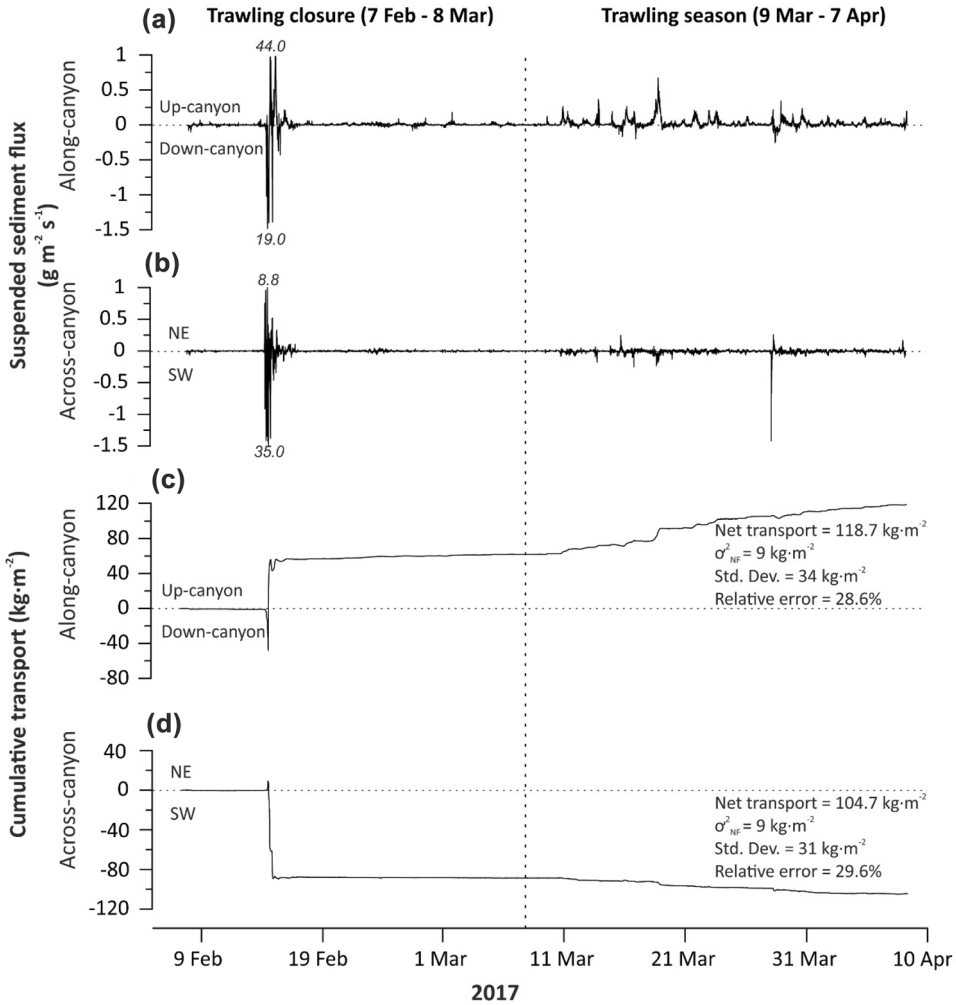

Fig. 11 **a** Instantaneous along-canyon suspended sediment flux (g m^{-2} s^{-1}), **b** instantaneous across-canyon suspended sediment flux (g m^{-2} s^{-1}), **c** along-canyon cumulative transport (kg m^{-2}) and **d** across-canyon cumulative transport (kg m^{-2}) at the mooring site during the monitoring period. Maximum sediment fluxes reached during DSWC events are indicated in italics. The dashed line separates the trawling closure from the trawling season. Inset on panels **c** and **d** provides the time-integrated cumulative transport (net transport) for the along- and across-canyon components and their uncertainty (σ^2_{NF}), the standard deviation and the relative error derived from these calculations for the entire monitoring period

Although relatively high SSC increases were recorded at intermediate water depths (> 3.5 mg L^{-1}) (Fig. 7c), very strong SSC increases (> 200 mg L^{-1}) occurred near the bottom (Fig. 7e). This indicates that the cascade of DSW during this event caused a rapid advection of cold and turbid waters down to the deepest part of the surveyed water column, presumably transporting easily erodible sediment particles on their way as they moved down-canyon, generating high near-bottom suspended sediment fluxes (Fig. 11a, b; Table 2). Previously recorded DSWC events in Palamós Canyon by Ribó et al. (2011) were specific for the canyon head (325 m depth) and accounted for lower down-canyon current velocities (> 0.4 m s^{-1} versus 0.6 m s^{-1}) and lower SSC peaks (~ 6 mg L^{-1} versus > 200 mg L^{-1}) than in the canyon axis. However, DSWC events of similar magnitude to that observed during the present study have been recorded in the Cap de Creus Canyon, where near-bottom

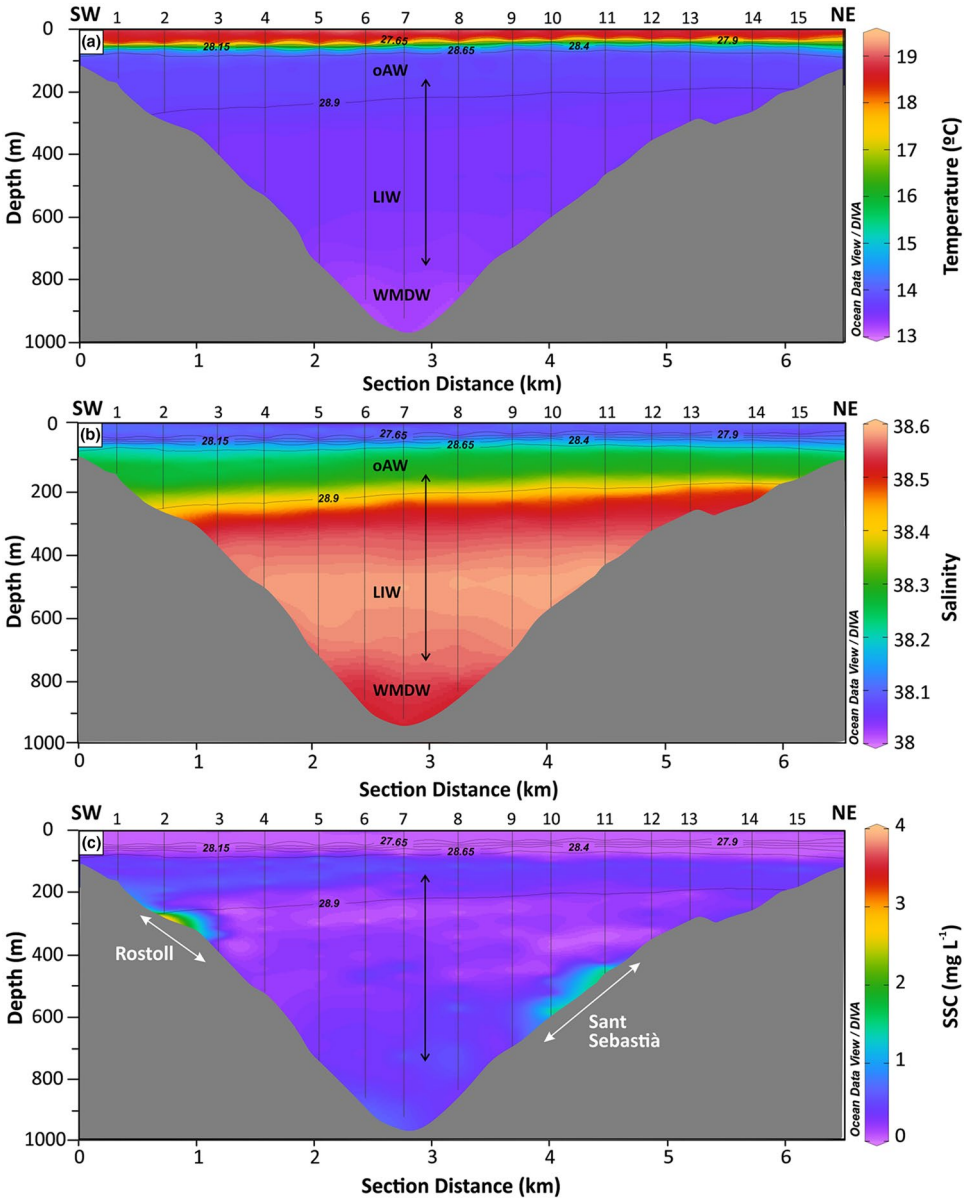

Fig. 12 CTD transect conducted in June 7, 2017 across the Palamós Canyon showing the distribution of **a** potential temperature (ºC), **b** salinity, with the different water masses present in the study area (see Fig. 5 for details), and **c** suspended sediment concentration (SSC, mg L^{-1}). The black arrow indicates the working depth range of the autonomous hydrographic profiler (Aqualog) and the white arrows indicate the bathymetric range occupied by the Sant Sebastià and Rostoll fishing grounds extracted from the AIS spatial distribution at the location where the CTD transect was conducted (see location in Fig. 2). For interpretation of the references in color in this figure legend, the reader is referred to the web version of this article

SSC > 170 mg L^{-1} and currents of ~0.6 m s^{-1} were registered (Ribó et al. 2011).

During the first stages of the major DSWC event recorded during the study, the near-bottom suspended sediment fluxes were mainly directed down-canyon and towards the SW (Fig. 11a, b), suggesting the arrival of a non-channeled cascade coming predominantly from the northern canyon flank. As the dominant eastern field veered to south-westerlies (not shown) and the storm ceased (Fig. 5b), currents inside the canyon reversed from down-canyon to up-canyon, peaking up to 0.6 m s^{-1} (Fig. 10b), and the DSW turbid plume was retained within the canyon's interior, increasing near-bottom SSC up to ~234 mg L^{-1} (Fig. 10d), generating an abrupt peak in near-bottom suspended sediment flux of 44 g m^{-2} s^{-1} directed up-canyon (Fig. 11a). This sudden change in current flow, due to the compensation of the isopycnals, has been previously described as the reversal (relaxation) phase of cascading/downwelling events (Ulses et al. 2008b), and described in detail in the Cap de Creus Canyon during a similar storm event in winter 2011 (Martín et al. 2013). The second DSW pulse detected on February 21 was not associated to any storm event nor a flashflood river discharge (Fig. 5), and in contrast to the first DSW pulse, it was shorter and only reached about 200 m depth (Fig. 7). This event generated lower SSC at the upper part of the hydrographic profiles, and no signal was recorded in the near-bottom instrumentation (Fig. 7). This mild and shallow DSW pulse was therefore smaller in magnitude and resembled those recorded at similar depths (~300 m depth) in this submarine canyon by Ribó et al. (2011).

During the trawling closure period, the presence of the WIW was detected at the hydrographic profiles reaching maximum water depths of ~400 m, alongside with relatively high SSC values in the profiled water column (Fig. 7a–c). The WIW observed during the study period could have been formed earlier during the winter season by DSWC events affecting the upper slope of the GoL (Lapouyade and Durrieu de Madron 2001; Dufau-Julliand et al. 2004; Durrieu de Madron et al. 2005a). This seasonal water mass could have then been advected southwards towards the Palamós Canyon, following the general circulation, and carrying an increased SSC signature. These high turbidity values, alongside with the increased SSC associated with the two DSW pulses, were also translated into higher NPSC during this period (Fig. 8a). Towards the end of the trawling closure period, the presence of waters generated by cooling and densification during winter (WIW and DSW) was no longer detected along the hydrographic profiles, and water turbidity decreased to almost baseline SSCs and NPSC in the upper water column, reaching the lowest values in the entire record (Figs. 7 and 8a).

Trawling-induced water turbidity and sediment transport

Considering the absence of major storm or flooding events during the trawling season (Fig. 5) and the position of OTB vessels and number of daily hauls (Figs. 2 and 4), we can infer that the occurrence of frequent events of increased water turbidity within the Palamós Canyon (Fig. 7c) was induced by the passage of OTB vessels along the canyon flanks.

Throughout the monitored trawling season, the more intense fishing activity was particularly detected at depths between 250 and 600 m at the southern canyon wall (Rostoll fishing ground), and between 400 and 800 m depth at the northern canyon wall (Sant Sebastià fishing ground) (Fig. 2). Based on the relative depths at which the trawling activities occur on each flank next to the mooring location, the shallower INLs (250–350 m water depth) observed in the hydrographic profiles and the CTD transect most probably correspond to resuspended sediment detached from the Rostoll fishing ground, whereas most of the SSC increases detected below 500 m depth could correspond to resuspension from the Sant Sebastià fishing ground (Figs. 7c and 12c). These well-developed INLs and BNLs detected at depths > 500 m are in agreement with previous observations reported by Martín et al. (2014a). In their study, a hydrographic transect conducted across the Sant Sebastià fishing ground revealed the presence of enhanced INLs and BNLs coinciding with the depth range exploited by otter trawlers. The higher number of hauls carried out at this fishing ground in contrast with the lower number of hauls occurring at the Rostoll fishing ground (Fig. 4) suggest that

Table 2 Near-bottom instantaneous suspended sediment (SS) fluxes (g m^{-2} s^{-1}) and cumulative transport (T m^{-2}) calculated for the along- and across-canyon components during the trawling closure, which includes the DSWC period, and the trawling season. For the along-canyon component up-canyon flux values and cumulative transport are positive, whereas for the down-canyon flux they are negative. For the across-canyon component NE orientation flux values are positive, whereas for the SW orientation they are negative

	Instantaneous SS flux		Cumulative transport	
	Along-canyon	Across-canyon	Along-canyon	Across-canyon
Trawling closure	0.02–0.1	0.01–0.06	+0.05	− 0.08
DSWC period (max.)	+44	− 35		
Trawling season	0.1–0.7	1.4	+0.04	− 0.02

most of the increases in water turbidity during the trawling season were generated in the northern canyon wall. Moreover, the Sant Sebastià fishing ground is closer to the canyon axis (~ 1.5 km) than the Rostoll fishing ground (~ 2.5 km), which would favor that most of SSC increases reaching the mooring location were detached from the northern canyon wall as nepheloid layers. Over this period, near-bottom suspended sediment fluxes presented a dominant direction towards the SW (Fig. 11b; Table 2), following the main flow of the geostrophic circulation in this margin, which also suggests that most the resuspended sediment came from the northern flank. Nonetheless, the time-integrated near-bottom cumulative transport over the trawling period showed a persistently up-canyon direction (Fig. 11c; Table 2). This fact seems to confirm previous time series observations within the Palamós Canyon, revealing the presence of a residual up-canyon flux superimposed to the periodical (i.e. inertial) up- and down-canyon flow oscillations along the canyon axis (Martín et al. 2006, 2007). This has important implications for the redistribution and final fate of bottom trawling resuspended sediments in the canyon, as sediment transported down-slope from the canyon flanks' fishing grounds would be retained by the up-canyon residual flow and rapidly deposited along the canyon axis, without being exported further down-canyon towards greater depths. This continuous up-canyon cumulative transport (Fig. 11c) may also explain the increase of sediment accumulation rates in Palamós Canyon (Martín et al. 2008; Puig et al. 2015), a phenomenon observed in other trawled submarine canyons of this margin (Paradis et al. 2017, 2018a, b), leading to the formation of canyon axes' anthropogenic depocenters next to trawling grounds.

The quasi-permanent presence of INLs and near-BNLs near the fishing grounds in the Palamós Canyon during the monitored trawling season (Fig. 7) resembles the nepheloid structure linked to the trawling activities at the fishing grounds of the Foix Canyon (Arjona-Camas et al. 2019). Both submarine canyons are deeply incised in the Catalan continental margin, at a relatively close distance from the coast and are affected differently by the corresponding bottom trawling fleets that operate on them. Trawling activities at the Foix Canyon take place along the canyon axis at 600–800 m depth, and mainly over the upper slope next to the canyon (200–500 m depth) (Lleonart 1990), from where resuspended particles are advected along-margin by ambient currents and cross over the canyon via nepheloid layers (Arjona-Camas et al. 2019). In contrast, trawling activities at the Palamós Canyon are not carried out along its axis, and occur mainly at the canyon flanks, with minimal activity on the northern upper slope (Figs. 2 and 4). Nevertheless, the few hauls carried out at the upper slope of the Palamós Canyon could have contributed to feed the particulate matter detachments observed between 90 and 200 m depth during the CTD transect conducted on June 7 (Fig. 12c), which generated an INL too shallow to be recorded by the moored instruments. The pycnocline between the oAW and the LIW (Fig. 12a, b) could have favored the retention of suspended particles at this depth range, which are advected towards the southwest by the geostrophic circulation, above the profiling range of the moored instruments (Fig. 7). Nevertheless, despite the different locations where trawling activities take place at the Foix and the Palamós submarine canyons, the nepheloid structure developed in both canyons is remarkably similar (see Fig. 6 in Arjona-Camas et al. 2019).

Overall, these new data from the Palamós Canyon supports the hypothesis that resuspension induced by bottom trawling activities can play a significant role in increasing SSC in the water column and generating INLs and BNLs at certain depths based on the locations of the fishing grounds. No other submarine canyon has been studied as intensively as the Palamós Canyon regarding the effects of bottom trawling on the sediment dynamics but given that canyons are very often targeted by demersal fisheries, it is likely that similar impacts have occurred and are occurring in other submarine canyons elsewhere. Similar enhanced trawling-induced nepheloid layers such as those reported in the present study at the Palamós Canyon and at the Foix Canyon by Arjona-Camas et al. (2019), have been reported in Whittard Canyon (NE Atlantic) (Wilson et al. 2015b; Daly et al. 2018). As discussed by Wilson et al. (2015b), although the trawling activity was not always adjacent to where these enhanced nepheloid layers were observed, the canyon would have likely transported the material down to deeper regions. However, due to limited dataset consisting in discrete CTD casts, these authors were not able to conclude the frequency of these events, nor their temporal evolution during the active trawling period at the Whittard Canyon (Wilson et al. 2015b).

Comparison between water turbidity during the trawling closure and the trawling season

Remarkable aspects during the trawling closure in February 2017 were the high SSC increases related to the two DSWC events in the canyon (Fig. 7), and the relatively high SSC values at the upper levels of the water column associated with the presence of WIW (Figs. 6 and 7). This generated high NPSC values computed for the upper levels of the profiled water column (Fig. 8a). By the end of the trawling closure period, water turbidity, as well as computed NPSC, decreased to baseline values (Figs. 7 and 8a), coinciding with the disappearance of the seasonal WIW and the subsequent reestablishment of the more general hydrographic structure of this region (Figs. 6 and 7a and b). As it has been previously stated, the formation of WIW over

the GoL is directly affected by strong atmospheric events (Duffau-Julliand et al. 2004; Juza et al. 2019), being especially intense between late January to early March. However, changes in these atmospheric forcing and/or inflowing of AW and water properties including changes in LIW, can affect its horizontal advection and mixing with surrounding waters (Juza et al. 2019) and, subsequently, control its presence within the Palamós Canyon. These multiple factors could explain the rapid disappearance of the WIW from the hydrographic profiles by the end of the trawling closure season (Fig. 7a, b).

During the trawling season, almost all increases in water turbidity were associated with the trawling activities in the study area. This was translated in higher NPSC during the trawling season, which were almost two times those calculated at the end of the trawling closure (Fig. 8a). This was not only observed in the upper water column NPSC water column inventories, which allowed us to compare both periods, but also in the entire profiled water column (Fig. 8b). The higher values calculated for the trawling season indicate that trawling can more than double the suspended sediment load in the water column, which is in agreement with suspended sediment inventories previously documented in other trawling grounds, both in shallow and deep-water environments (Palanques et al. 2001, 2014; Arjona-Camas et al. 2019). Suspended sediment concentrations in the water column did not vary significantly when the trawling fleet was not operating on weekends and holidays at the flanks of the canyon. These results contrast with previous observations from a canyon tributary next to the Sant Sebastià fishing ground, which documented the occurrence of frequent events of high turbidity (i.e., sediment gravity flows) during working days and working hours of the local trawling fleet (Palanques et al. 2006a; Puig et al. 2012; Martín et al. 2014a). Additionally, this data showed that these events occurred once or twice a day when the trawling fleet went offshore and when it headed back to port (Martín et al. 2014a). However, in the present study the near-bottom time series collected at 923 m depth in the canyon axis did not record such periodic sediment gravity flows events (Figs. 7 and 10), as the instruments of the mooring were not receiving channeled trawled resuspended sediment through any canyon tributary. Instead, they received the less dense sediment particles that were scattered from the trawling grounds and remained in suspension after the passage of the sediment gravity flows. Once particles were detached in the water column, they remained in suspension for long periods of time, contributing to feed quasi-permanent INLs and BNLs, where SSC was higher. Because of this, these increases of SSC did not show differences between working days and weekends.

Conclusions

The data recorded in this monitoring study show different turbidity and sediment transport patterns between the trawling closure period and the trawling season at the Palamós Canyon.

During the trawling closure period, natural increases in water turbidity and near-bottom suspended sediment fluxes occurred mainly during DSWC events. These observations provided further insight of the sediment transport associated with this oceanographic process in Palamós Canyon and showed evidence, for the first time, of the presence of DSWC reaching > 900 m depth in the canyon axis. During the trawling season, increases in water turbidity linked to trawling activities occurred regularly and were recorded mainly concentrated at depths where the Sant Sebastià and the Rostoll fishing grounds are located. Bottom trawling introduced sediment into the water column that more than doubled the suspended sediment background values recorded during calm sea conditions of the trawling closure, in absence of dense shelf waters within the canyon. Near-bottom instantaneous suspended sediment fluxes caused by the passage of OTB vessels were some orders of magnitude smaller than those generated by DSWC events. However, the chronic trawling activities for at least 30 days over the same fishing ground are capable of producing similar cumulative suspended sediment transport to that generated by a major DSWC event.

The main difference between natural and trawling-induced mechanisms is that natural turbidity and suspended sediment transport occurs sporadically, whereas trawling-induced water turbidity and transport is periodic and constant. Taking into account that bottom trawling is practiced on a daily basis throughout the year at the flanks of Palamós Canyon, with the exception of the 60-day seasonal trawling closure, weekends and holidays, much higher suspended sediment transport would be expected for a complete trawling season. Results from this study provide further insight on how bottom trawling activities are able to overcome natural processes as the main mechanism of sediment resuspension, capable of changing the natural patterns of particulate matter dispersion and accumulation in submarine canyon environments.

The capacity of bottom trawling to produce similar accumulated impacts to those resulting from sudden and sporadic natural high-energy events points out the necessity of addressing the effect of anthropogenic activities in studies of sediment dynamics in deep-sea environments where fishing activities are practiced.

Further mooring data in this and other submarine canyons, along with data on the composition of the sediment resuspended by both natural and trawling-induced mechanisms would provide additional data on the biogeochemical

and ecological consequences derived from this human activity.

Acknowledgements The authors are very grateful to the captain, crew and scientists involved in R/V *García del Cid* cruises, and to the UTM technicians and the Instrumental Service for their guidance and assistance. The authors wish to thank the Secretaría General de Pesca (SGP) for providing the 2004 Espace Project bathymetry and the Spanish Ports Authority for the access to AIS data. This work has been supported by the ABIDES (CTM2015-65142) Spanish Project and by the autonomous government of Catalonia grants 2017 SGR 863 and 2017 SGR 1241, as well as by the TrawledSeas Project receiving funding from the European Union's Horizon 2020 Research and Innovation programme under a MSCA grant agreement (No. 867471). M. Arjona-Camas is supported by a predoctoral FPI grant from the Spanish Ministry of Economy, Industry and Competitiveness.

Author contributions MAC: methodology, software, visualization, datacuration, formal analysis, writing. PP: conceptualization, funding acquisition, reviewing and editing, supervision. AP: funding acquisition, reviewing and editing, supervision. RD: software, visualization. MW: formal analysis. SP: methodology, software, data curation. ME: methodology, formal analysis, visualization.

References

Allen SE, Durrieu de Madron X (2009) A review of the role of submarine canyons in deep-ocean exchange with the shelf. Ocean Sci 5(4):607

Amblas D, Canals M, Urgeles R, Lastras G, Liquete C, Hughes-Clarke JE, Casamor JL, Calafat AM (2006) Morphogenetic mesoscale analysis of the northeastern Iberian margin, NW Mediterranean Basin. Mar Geol 234(1–4):3–20

Arjona-Camas M, Puig P, Palanques A, Emelianov M, Durán R (2019) Evidence of trawling-induced resuspension events in the generation of nepheloid layers in the Foix submarine canyon (NW Mediterranean). J Mar Syst 196:86–96

Bjørkan M, Company JB, Gorelli G, Sardà F, Massaguer C (2020) When fishemen take charge: the development of a management plan for the red shrimp fishery in Mediterranean Sea (NE Spain). Springer, Cham, pp 159–178

BOE (2017) Resolución de 26 de enero de 2017, de la Secretaría General de Pesca, por la que se fija, para 2017, el periodo de veda establecido en la Orden AAA/923/2013, de 16 de mayo, por la que se regula la pesca de gamba rosada (Aristeus antennatus) con arte de arrastre de fondo en determinadas zonas marítimas próximas a Palamós

Bonnin J, Heussner S, Calafat A, Fabres J, Palanques A, Durrieu de Madron X, Canals M, Puig P, Avril J, Delsaut N (2008) Comparison of horizontal and downward particle fluxes across canyons of the Gulf of Lions (NW Mediterranean): meteorological and hydrodynamical forcing. Cont Shelf Res 28(15):1957–1970

Cacchione DA, Pratson LF, Ogston AS (2002) The shaping of continental slopes by internal tides. Science 296(5568):724–727

Canals M, Puig P, Durrieu de Madron X, Heussner S, Palanques A, Fabres J (2006) Flushing and reshaping submarine canyons by dense shelf water cascading. Nature 444(7117):354–357

Canals M, Company JB, Martín D, Sanchez-Vidal A, Ramirez-Llodra E (2013) Integrated study of Mediterranean deep canyons. Novel results and future challenges. Prog Oceanogr 118:1–27

Churchill JH (1989) The effect of commercial trawling on sediment resuspension and transport over the Middle Atlantic Bight continental shelf. Cont Shelf Res 9(9):841–865

Daly E, Johnson MP, Wilson AM, Gerritsen HD, Kiriakoulakis K, Allcock AL, White M (2018) Bottom trawling at Whittard Canyon: evidence for seabed modification, trawl plumes and food source heterogeneity. Progr Oceanogr 169:227–240

Dufau-Julliand C, Marsaleix P, Petrenko A, Dekeyser I (2004) Three-dimensional modeling of the Gulf of Lion's hydrodynamics (northwest Mediterranean) during January 1999 (MOOGLI3 experiment) and late winter 1999: western Mediterranean Intermediate Water's (WIW's) formation and its cascading over the shelf break. J Geophys Res 109(C1):1002

Durrieu de Madron, X, Zervakis V, Theocharis A, Georgopoulos D (2005a) Comments on ''Cascades of dense water around the world ocean''. Prog Oceanogr 64(1):83–90

Durrieu de Madron X, Ferré B, Le Corre G, Grenz C, Conan P, Pujo-Pay M, Buscail R, Bodiot O (2005b) Trawling-induced resuspension and dispersal of muddy sediments and dissolved elements in the Gulf of Lion (NW Mediterranean). Cont Shelf Res 25:2387–2409

Durrieu de Madron, X, Houpert L, Puig P, Sanchez-Vidal A, Testor P, Bosse A, Estournel C, Somot S, Bourrin F, Bouin MN, Beauverger M, Beguery L, Calafat A, Canals M, Coppola L, Dausse D, D'Ortenzio F, Font J, Heussner S, Kunesch S, Lefevre D, Le Goff H, Martín J, Mortier L, Palanques A, Raimbault P (2013) Interaction of dense shelf water cascading and open-sea convection in the Northwestern Mediterranean during winter 2012. Geophys Res Lett 40:1379–1385

European Commission Fisheries & Maritime Affairs (2014) Fleet register on the net. http://ec.europa.eu/fisheries/fleet/index.cfm. Accessed 1 Apr 2019

Ferré B, de Madron D, Estournel X, Ulses C, Le Corre C, G (2008) Impacto f natural (waves and currents) and anthropogenic (trawl) resuspension on the export of particulate matter to the open ocean: application to the Gulf of Lion (NW Mediterranean). Cont Shelf Res 28(15):2071–2091

Font J, Salat J, Tintoré J (1988) Permanent features of the circulation in the Catalan Sea. Ocenol Acta 9:51–57

Font J, Puig P, Salat J, Palanques A, Emelianov M (2007) Sequence of hydrographic changes in the NW Mediterranean deep water due to the exceptional winter of 2005. Sci Mar 71:339–346

García R, Van Oevelen D, Soetaert K, Thomsen L, De Stigter HC, Epping E (2008) Deposition rates, mixing intensity and organic content in two contrasting submarine canyons. Prog Oceanogr 76(2):192–215

Gardner WD (1989) Baltimore canyon as a modern conduit of sediment to the deep sea. Deep-Sea Res 36:323–358

Guillén J, Bourrin F, Palanques A, Durrieu de Madron XD, Puig P, Buscail R (2006) Sediment dynamics during wet and dry storm events on the Têt inner shelf (SW Gulf of Lions). Mar Geol 234:129–142

Harris PT, Whiteway T (2011) Global distribution of large submarine canyons: geomorphic differences between active and passive continental margins. Mar Geol 285:69–86

Jordi A, Orfila A, Basterretxea G, Tintoré J (2005) Shelf-slope exchanges by frontal variability in a steep submarine canyon. Prog Oceanogr 6:120–141

Juza M, Escudier R, Vargas-Yáñez M, Mourre B, Heslop E, Allen J, Tintoré J (2019) Characterization of changes in western intermediate water properties enabled by an innovative geometry-based detection approach. J Mar Sys 191:1–12

Karageorgis AP, Anagnostou CL (2003) Seasonal variation in the distribution of suspended particulate matter in the northwest Aegean Sea. J Geophys Res Oceans 108(C8):3274

Krost P, Bernhard M, Werner F, Hukriede W (1990) Otter-trawl tracks in Kiel Bay (Western Baltic) mapped by side-scan sonar. Meeresforsch 32(4):344–353

Kunze E, Rosenfeld LK, Carter GS, Gregg MC (2002) Internal waves in Monterey submarine canyon. J Phys Oceanogr 32(6):1890–1913

Lapouyade A, Durrieu de Madron X (2001) Seasonal variability of the advective transport of particulate matter and organic carbon in the Gulf of Lion (NW Mediterranean). Oceanol Acta 24:295–312

Lastras G, Canals M, Amblas D, Lavoie C, Church I, De Mol B, Duran R, Calafat AM, Hughes-Clarke JE, Smith CJ, Heussner S, "Euroléon" cruise shipboard party (2011) Understanding sediment dynamics in two large submarine valleys from seafloor data: Blanes and La Fonera canyons, northwestern Mediterranean Sea. Mar Geol 280(1–4):20–39

Liquete C, Canals M, Ludwig W, Arnau P (2009) Sediment discharge of the rivers of Catalonia, NE Spain, and the influence of human impacts. J Hydrol 366(1–4):76–88

Lleonart J (1990) La pesquería de Cataluña y Valencia: descripción global y planteamiento de bases para su seguimiento. (Informe final. EEC DG XP/-CSIC, 2)

Martín J, Palanques A, Puig P (2006) Composition and variability of downward particulate matter fluxes in Palamós submarine canyon (NW Mediterranean). J Mar Sys 60:75–97

Martín J, Palanques A, Puig P (2007) Near-bottom horizontal transfer of particulate matter in the Palamós submarine canyon (NW Mediterranean). J Mar Res 65(2):193–218

Martín J, Puig P, Palanques A, Masqué P, García-Orellana J (2008) Effect of commercial trawling on the deep sedimentation in a Mediterranean submarine canyon. Mar Geol 252(3–4):150–155

Martín J, Durrieu de Madron X, Puig P, Bourrin F, Palanques A, Houpert L, Higueras M, Sanchez-Vidal A, Calafat AM, Canals M, Heussner S, Delsaut N, Sotin C (2013) Sediment transport along the Cap de Creus canyon flank during a mild, wet winter. Biogeosciences 10(5):3221–3239

Martín J, Puig P, Palanques A, Ribo M (2014a) Trawling-induced daily sediment resuspension in the flank of a Mediterranean submarine canyon. Deep-Sea Res II Top Stud Oceanogr 104:174–183

Martín J, Puig P, Masqué P, Palanques A, Sánchez-Gómez A (2014b) Impact of bottom trawling on deep-sea sediment properties along the flanks of a submarine canyon. PLoS One 9(8):e104536

Masó M, Tintoré J (1991) Variability of the shelf water off the northeast Spanish coast. J Mar Sys 1(4):441–450

Mendoza ET, Jiménez AA (2009) Vulnerability assessment to coastal storms at a regional scale. In: Coastal engineering 2008, vol 5, pp 4154–4166

Mengual B, Cayocca F, Le Hir P, Draye R, Laffargue P, Vincent B, Garlan T (2016) Influence of bottom trawling on sediment resuspension in the 'Grande-Vasière'area (Bay of Biscay, France). Ocean Dyn 66(9):1181–1207

Millot C (1990) The Gulf of Lions' hydrodynamics. Cont Shelf Res 10(9–11):885–894

Millot C (1999) Circulation in the Western Mediterranean Sea. J Mar Sys 20:423–442

Monaco A, Biscaye PE, Soyer J, Pocklington R, Heussner S (1990) Particle fluxes and ecosystem response on a continental margin: the 1985–1988 Mediterranean ECOMARGE experiment. Cont Shelf Res 10:809–839

Natale F, Gibin M, Alessandrini A, Vespe M, Paulrud A (2015) Mapping fishing effort through AIS Data. PloS One 10(6):e0130746

Oberle FKJ, Storlazzi CD, Hanebuth TJJ (2016) What a drag: quantifying the global impact of chronic bottom trawling on continental shelf sediment. J Mar Syst 159:109–119

O'Neill FG, Summerbell K (2011) The mobilisation of sediment by demersal otter trawls. Mar Pollut Bull 62(5):1088–1097

Palanques A, Guillén J, Puig P (2001) Impact of bottom trawling on water turbidity and muddy sediment of an unfished Impact of bottom trawling continental shelf. Limnol Oceanogr 46:1100–1110

Palanques A, García-Ladona E, Gomis D, Martín J, Marcos M, Pascual A, Puig P, Gili JM, Emelianov M, Monserrat S, Guillén J, Tintoré J, Segura M, Jordi A, Ruiz S, Basterretxea G, Font J, Blasco D, Pagès F (2005) General patterns of circulation, sediment fluxes and ecology of the Palamós (La Fonera) submarine canyon, northwestern Mediterranean. Prog Oceanogr 66(2–4):89–119

Palanques A, Martín J, Puig P, Guillén J, Company JB, Sardà F (2006a) Evidence of sediment gravity flows induced by trawling in the Palamós (Fonera) submarine canyon (northwestern Mediterranean). Deep-Sea Res Part I Oceanogr Res Pap 53(2):201–214

Palanques A, Durrieu de Madron X, Puig P, Fabres J, Guillén J, Calafat A, Canals M, Bonnin J (2006b) Suspended sediment fluxes and transport processes in the Gulf of Lions submarine canyons: the role of storms and dense shelf water cascading. Mar Geol 234(1–4):43–61

Palanques A, Guillén J, Puig P, Durrieu de Madron X (2008) Storm-driven shelf-to-canyon suspended sediment transport at the southwestern Gulf of Lions. Cont Shelf Res 28(15):1947–1956

Palanques A, Puig P, Durrieu de Madron X, Sanchez-Vidal A, Pasqual C, Martín J, Calafat A, Heussner S, Canals M (2012) Sediment transport to the deep canyons and open-slope of the western Gulf of Lions during the 2006 intense cascading and open-sea convection period. Prog Oceanogr 106:1–15

Palanques A, Puig P, Guillén J, Demestre M, Martín J (2014) Effects of bottom trawling on the Ebro continental shelf sedimentary system (NW Mediterranean). Cont Shelf Res 72:83–98

Palanques A, Puig P (2018) Particle fluxes induced by benthic storms during the 2012 dense shelf water cascading and open sea convection period in the northwestern Mediterranean basin. Mar Geol 406:119–131

Paradis S, Puig P, Masqué P, Juan-Díaz X, Martín J, Palanques A (2017) Bottom trawling along submarine canyons impacts deep sedimentary regimes. Sci Rep 7:43332

Paradis S, Puig P, Sánchez-Vidal A, Masqué P, García-Orellana J, Calafat A, Canals M (2018a) Spatial distribution of sedimentation-rate increases in Blanes canyon caused by technification of bottom trawling fleet. Prog Oceanogr 169:241–252

Paradis S, Masqué P, Puig P, Juan-Díaz X, Gorelli G, Palanques A (2018b) Enhancement of sedimentation rates in the Foix canyon after the renewal of trawling fleets in the early XXI st century. Deep-Sea Res I Oceanogr Res Pap 132:51–59

Paradis S, Goñi M, Masqué P, Durán R, Arjona-Camas M, Palanques A, Puig P (2021) Persistence of biogeochemical alterations of deep-sea sediments by bottom trawling. Geophys Res Lett 48:e2020GL091279

Paull CK, Ussler W, Greene HG, Keaten R, Mitts P, Barry J (2003) Caught in the act: the 20 December 2001 gravity flow event in Monterey canyon. Geo-Mar Lett 22(4):227–232

Payo-Payo M, Jacinto RS, Lastras G, Rabineau M, Puig P, Martín J, Canals M, Sultan N (2017) Numerical modeling of bottom trawling-induced sediment transport and accumulation in La Fonera submarine canyon, northwestern Mediterranean Sea. Mar Geol 386:107–125

Pilskaln CH, Churchill JH, Mayer LM (1998) Resuspension of sediment by bottom trawling in the Gulf of Maine and sediment potential geochemical consequences. Conserv Biol 12(6):1223–1229

Piper DJW, Normark WR (2009) Processes that initiate turbidity currents and their influence on turbidites: a marine geology perspective. J Sediment Res 79(6):347–362

Pomar L, Morsili M, Hallock P, Bádenas B (2012) Internal waves, an under-explored source of turbulence events in the sedimentary record. Earth Sci Rev 111:56–81

Porter M, Inall ME, Hopkins J, Palmer MR, Dale AC, Barth JA, Mahaffey C, Smeed DA (2016) Glider observations of enhanced deep water upwelling at a shelf break canyon: a mechanism for cross-slope carbon and nutrient. J Geophys Res Oceans 121:7575–7588

Puertos del Estado, ShipLocus (2017). https://shiplocus.puertos.es/. Accessed 1 Jan 2018

Puig P, Palanques A (1998b) Temporal variability and composition of settling particle fluxes on the Barcelona continental margin (Northwestern Mediterranean). J Mar Res 56:639–654

Puig P, Ogston AS, Mullenbach BL, Nittrouer CA, Sternberg RW (2003) Shelf-to-canyon sediment-transport processes on the Eel continental margin (northern California). Mar Geol 193(1–2):129–149

Puig P, Ogston AS, Mullenbach BL, Nittrouer CA, Parsons JD, Sternberg RW (2004a) Storm-induced sediment gravity flows at the head of the Eel submarine canyon, northern California margin. J Geophys Res 109(C3):C03019

Puig P, Palanques A, Guillén J, Khatab E, M (2004b) Role of internal waves in the generation of nepheloid layers on the northwestern Alboran slope: implications for continental margin shaping. J Geophys Res-Oceans 109:C9

Puig P, Palanques A, Orange DL, Lastras G, Canals M (2008) Dense shelf water cascades and sedimentary furrow formation in the Cap de Creus canyon, northwestern Mediterranean Sea. Cont Shelf Res 28(15):2017–2030

Puig P, Canals M, Martín J, Amblas D, Lastras G, Palanques A, Calafat A (2012) Ploughing the deep-sea floor. Nature 489(7415):286

Puig P, Palanques A, Martín J (2014) Contemporary sediment-transport processes in submarine canyons. Annu Rev Mar Sci 6:53–77

Puig P, Martín J, Masqué P, Palanques A (2015) Increasing sediment accumulation rates in La Fonera (Palamós) submarine canyon axis and their relationship with bottom trawling activities. Geophys Res Lett 42:8106–8113

Ragnarsson S, Steingrímsson SA (2003) Spatial distribution of otter trawl effort on Icelandic waters: comparison of measures of effort and implications for benthic community effects of trawling activities. ICES J Mar Sci 60(6):1200–1215

Ribó M, Puig P, Palanques A, Lo Iacono C (2011) Dense shelf water cascades in the Cap de Creus and Palamós submarine canyons during winter 2007 and 2008. Mar Geol 284:175–188

Salat J, Cruzado A (1981) Water masses in the Western Mediterranean Sea: Catalan Sea and adjacent waters. Rap Proc CIESM 27(6):6

Salat J, García MA, Cruzado A, Palanques A, Arín L, Gomis D, Guillén J, de León A, Puigdefàbregas J, Sospedra J, Velásquez ZR (2002) Seasonal changes of water mass structure and shelf slope exchanges at the Ebro shelf (NW Mediterranean). Cont Shelf Res 22:327–348

Serra J (1981) Els canyons submarins del marge Català. Treb Inst Cat Hist Nat 9:53–57

Shepard FP (1972) Submarine canyons. Earth Sci Rev 8(1):1–12

Shepard FP, Dill RF (1966) Submarine canyos and other sea valleys. Rand McNally, USA

Smith C, Rumohr H, Karakassis I, Papadopoulou KN (2003) Analysing the impact of bottom trawls on sedimentary seabeds with sediment profile imagery. J Exp Mar Biol Ecol 285:479–496

Ulses C, Estournel C, Durrieu de Madron X, Palanques A (2008a) Suspended sediment transport in the Gulf of Lions (NW Mediterranean): impact of extreme storms and floods. Cont Shelf Res 28(15):2048–2070

Ulses C, Estournel C, Bonnin J, Durrieu de Madron X, Marsaleix P (2008b) Impact of storms and dense water cascading on shelf-slope exchanges in the Gulf of Lion (NW Mediterranean). J Geophys Res 113:C02010

Völker D, Scholz F, Geersen J (2011) Analysis of submarine landsliding in the rupture area of the 27 February 2010 Maule earthquake, Central Chile. Mar Geol 288:79–89

Wilson AM, Kiriakoulakis K, Raine R, Gerritsen HD, Blackbird S, Allcock AL, White M (2015b) Anthropogenic influence on sediment transport in the Whittard Canyon, NE Atlantic. Mar Pollut Bull 101(1):320–329

Xu JP, Noble MA, Rosenfeld LK (2004) In-situ measurements of velocity structure within turbidity currents. Geophys Res Lett 31(9):L09311